Corresponding Author: Dr. Yu-ichiro Izato, Ph. D.

Corresponding Author's Institution: Yokohama National University

First Author: Yu-ichiro Izato, Ph. D.

Order of Authors: Yu-ichiro Izato, Ph. D.; Atsumi Miyake, Professor

Abstract: Ammonium dinitramide (ADN; $[NH4]^+[N(NO2)2]^-$) is the most promising oxidizer for use with future green solid and liquid propellants for spacecraft applications. To allow the effective development and use of ADN-based propellants, it is important to understand ADN reaction mechanisms. This work presents a detailed chemical kinetics model for the liquid phase reactions of ADN based on quantum chemical calculations. The thermal corrections, entropies, and heat capacities of chemical species were calculated from the partition function using statistical machinery based on the G4 level of theory. Rate coefficients were also determined to allow the application of transition state theory and variational transition state theory to reactions identified in our previous study. The new model employed herein simulates the thermal decomposition of ADN under specific heating conditions and successfully predicts heats of reaction and the gases that result from decomposition under those conditions. The thermal behaviour predicted from the new model was an excellent match with the experimental behaviour observed from thermal analysis using differential scanning calorimetry and Raman spectroscopy. The new kinetic model reveals the mechanism for the decomposition of ADN.

Detailed Kinetic Model for Ammonium Dinitramide Decomposition.

Authors   Yu-ichiro Izato [a] and Atsumi Miyake [b]

[a] Graduate school of environment and information sciences, Yokohama National University

79-7 Tokiwadai, Hodogaya-ku, Yokohama-shi 240-8501, JAPAN

[b] Institute of Advanced Sciences, Yokohama National University

79-5 Tokiwadai, Hodogaya-ku, Yokohama-shi 240-8501, JAPAN

Phone: +81-45-339-3981

Corresponding address: izato-yuichiro-hk@ynu.jp

Abstract

Ammonium dinitramide (ADN; $[NH_4]^+[N(NO_2)_2]^-$) is the most promising oxidizer for use

with future green solid and liquid propellants for spacecraft applications. To allow the

effective development and use of ADN-based propellants, it is important to understand ADN

reaction mechanisms. This work presents a detailed chemical kinetics model for the liquid

phase reactions of ADN based on quantum chemical calculations. The thermal corrections,

entropies, and heat capacities of chemical species were calculated from the partition function

using statistical machinery based on the G4 level of theory. Rate coefficients were also

determined to allow the application of transition state theory and variational transition state

theory to reactions identified in our previous study. The new model employed herein

simulates the thermal decomposition of ADN under specific heating conditions and

successfully predicts heats of reaction and the gases that result from decomposition under

those conditions. The thermal behaviour predicted from the new model was an excellent

match with the experimental behaviour observed from thermal analysis using differential

scanning calorimetry and Raman spectroscopy. The new kinetic model reveals the mechanism

for the decomposition of ADN.

2

kinetics

1. Introduction

Ammonium dinitramide (ADN; $NH_4N(NO_2)_2$) has attracted attention as a novel and

environmentally friendly solid/liquid propellant oxidizer because it possesses both a good

oxygen balance and a high energy content, and it does not contain halogen atoms [1-3].

Information regarding the decomposition and combustion behavior of propellant ingredients

such as ADN is useful when developing comprehensive ignition and combustion models for

rocket motors and gas generators that employ these materials. The combustion of energetic

salts, including ADN, is typically characterized by a diverse range of physical and chemical

processes that occur in a complex series of stages. In the case of ADN, the condensed phase

reactions have the greatest effect on the combustion characteristics [4-6]. Some reliable

energetic-salt gas-phase reaction models have been proposed to date, all of which work to

explain observed combustion behavior [4,7-9]. More recently, models for the liquid phase

reactions of these compounds have also been developed [10-14]. However, there are no

detailed reaction models for the condensed phase reactions of ADN, only semi-detailed

mechanisms [4].

    To construct a detailed reaction model for the condensed phase reactions of ADN, it is

3

important to understand the thermal decomposition pathways and the associated kinetics.

There have been many studies regarding the reaction mechanisms of ADN [15-19]. Yang et al.

[15] assessed ADN liquid phase decomposition and reported that it may proceed through one

of two competing mechanisms: ADN $\rightarrow$ NH_4NO_3 (AN; ammonium nitrate) + N_2O or ADN $\rightarrow$

NH_3 + HNO_3 + N_2O. The competing mechanisms in the gas phase are ADN $\rightarrow$ NH_3 +

dinitraminic acid (HDN) and ADN $\rightarrow$ NH_3 + HNO_3 + N_2O. However, in practice, it is

difficult to experimentally distinguish the latter reaction from the series consisting of ADN $\rightarrow$

NH_3 + HDN followed by HDN $\rightarrow$ N_2O + HNO_3, and to distinguish ADN $\rightarrow$ AN + N_2O from

the series of reactions ADN $\rightarrow$ NH_3 + HDN followed by HDN $\rightarrow$ N_2O + HNO_3 and NH_3 +

HNO_3 $\rightarrow$ AN. There have been several experimental studies on the kinetics of ADN

decomposition under various conditions [20-26] and the results have been summarized in

several publications [15,16].

In our previous work [27], quantum chemistry calculations that incorporated solvent effects

were used to investigate the decomposition pathways in aqueous ADN solutions. Optimized

structures for reactants and products were obtained at the CBS-QB3 [28]//ωB97X-D

[29]/6-311++G(d,p)/SCRF=(solvent=water) level of theory, considering the isomers ADN_I

(NH_4-$N(NO_2)_2$) and ADN_{II} (NH_4-ON(O)NNO$_2$), and the four ADN_{II} conformers. Although

ADN can potentially dissociate to either an anion-cation pair or an acid-base pair, the thermal

4

assessment in this study determined that ionization is preferable to acid-base dissociation in aqueous solution. In the initial stage of decomposition, the ADN_{II} conformers and the dinitraminic anion (DN^-) decompose to $NO_2\cdot$ and de-$NO_2\cdot$ intermediates (NNO_2NH_4 and NNO_2^-), while neither ADN_I nor dinitraminic acid plays an important role. Following the initial decomposition, $NNO_2NH_4\cdot$ and $NNO_2^-\cdot$ transition to $NNO_2H\cdot$ and NH_3 through proton transfer, after which the NNO_2H decomposes to N_2O and $OH\cdot$, and the $OH\cdot$ combines with $NO_2\cdot$ from the initial reaction to yield HNO_3. This decomposition can be expressed using one global formula: $ADN \rightarrow N_2O + NH_4NO_3$ ($NH_3 + HNO_3$).

The purpose of the present work is (i) to develop a detailed chemical model using kinetic data based on reactions identified in previous studies [24,25,27], (ii) to validate the model by comparison with data obtained from experimental thermal analysis and the literature [30], and (iii) to reveal the ADN decomposition mechanism theoretically.

2. Computational

2.1 Rate coefficients

The rate coefficient k_{TST}, for the generic reaction A + B $\rightarrow$ P (products in solution) can be calculated on the basis of traditional transition state theory (TST) using the formula

$$k_{TST} = \frac{k_B T}{h} \frac{Q_{TS}}{\prod Q_{reac}} \exp\left(\frac{-\Delta E_0}{RT}\right) \tag{1}$$

where k_B is the Boltzmann constant, T is the temperature, h is the Planck constant, Q_i is the

partition function of the reactant and transition state (TS), DE is the energy barrier to

activation, and R is the universal gas constant. Variational transition state theory (VTST) was

applied to analysis of the dissociation reactions without activation energy barriers. These

calculations were performed using the GPOP software package developed by Miyoshi [31].

The pressure dependence of rate for a monomolecular reaction in the gas phase must

generally be considered. However, in the liquid phase, a species is surrounded by many

species; i.e., the liquid state can be considered as a high-pressure condition. Thus, the rate at

the high-pressure limit was used for monomolecular reaction in the liquid phase. In our

previous work, liquid-phase calculations were performed at the CBS-QB3 [29]//ωB97X-D

[30]/6-311++G(d,p)/SCRF=(solvent=water) level of theory, and the associated potential

energy diagrams and TS structures were identified and investigated [24,25,27]. Radical

recombination and proton transfer with no barriers were simply modeled as diffusion-limited

reactions with the rate coefficient set at 10^{12} cm^3 mol^{-1} s^{-1}. This assumption is supported by

data from the aqueous kinetics database of the Notre Dame Radiation Laboratory, which

generally shows rate coefficients between 10^{12} and 10^{13} cm^3 mol^{-1} s^{-1} for radical

recombination reactions. The diffusivity-dependent encounter rate of two species and the

Stokes-Einstein diffusion within the solvent were used to estimate these rate coefficients

[12,32].

The important reactions associated with the decomposition of liquid phase ADN and the associated kinetic parameters for the modified Arrhenius equation are provided in Table 1.

This work investigated and modeled the thermal chemistry associated with the isomerization, conformational changes, and dissociation of ADN. Previous studies show that liquid ADN and HDN also have both an isomer and four conformers. In the present study, two liquid ADN isomers ($ADN_I = NH_4-N(NO_2)_2$ and $ADN_{II} = NH_4-ON(O)NNO_2$, Figure 1), two HDN isomers ($HDN_I = HN(NO_2)_2$ and $HDN_{II} = HON(O)NNO_2$, Figure 1), and the dinitraminic anion ($DN^- = N(NO_2)_2^-$) were also considered. It is noted that an ion in molten salt is surrounded by many counter ions. DN^- can be surrounded by several NH_4^+ ions and larger clusters including several ADN units can exist in molten ADN. Rahm and Brinck [33] investigated the thermal decomposition of solid-state ADN by the quantum chemical modeling of molecular clusters. In the present paper, only a minimal unit of ADN clusters (ADN_I and ADN_{II}) is of concern as the first step toward a deep understanding of the thermal decomposition of liquid-state ADN.
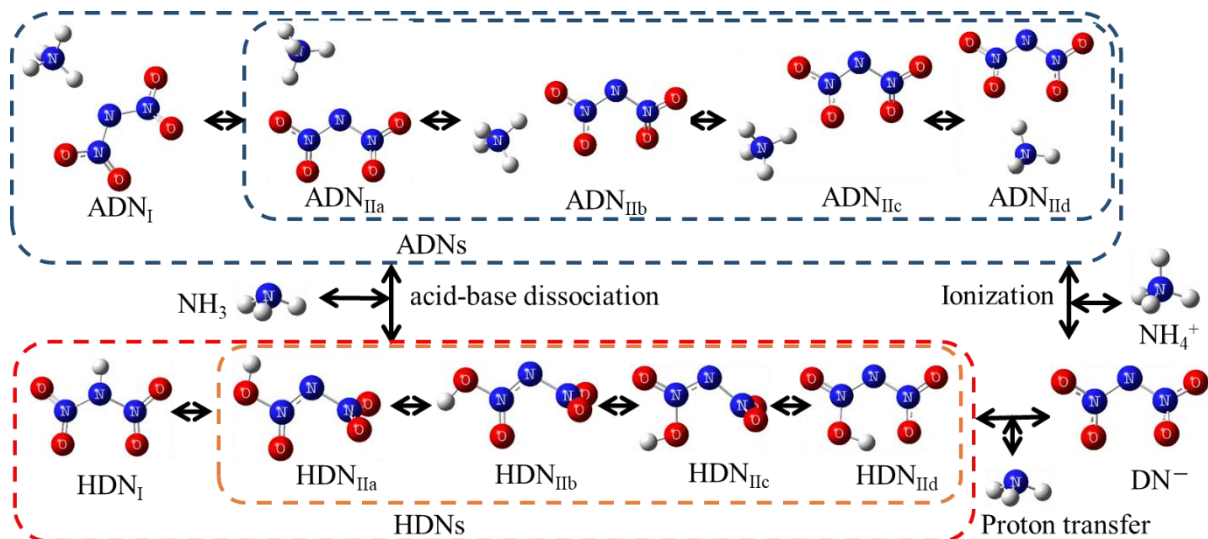
Figure 1. Chemical equilibrium diagram for ADN, HDN, and DN⁻ with structures optimized at the ωB97X-D/6-311++G(d,p)/SCRF=(solvent = water) level of theory.

Table 1. Reactions and rate coefficients employed during the kinetic modeling of ionic decomposition. units are in cm^3 mol s cal.

No.	Reaction	k		
		A	n	ΔE_a
1	$ADN_I \rightleftharpoons ADN_{IIa}$	2.06×10^{12}	0.04	1472
2	$ADN_{IIa} \rightleftharpoons ADN_{IIb}$	1.73×10^{12}	0.00	2420
3	$ADN_{IIb} \rightleftharpoons ADN_{IIc}$	4.58×10^{12}	0.03	1382
4	$ADN_{IIc} \rightleftharpoons ADN_{IId}$	1.86×10^{12}	0.01	2072
5	$ADN_{IIa} \rightleftharpoons NH_4^+ + DN^-$	1.06×10^{14}	-0.13	8671
6	$ADN_{IIb} \rightleftharpoons NH_4^+ + DN^-$	4.66×10^{13}	-0.07	8224
7	$ADN_{IIc} \rightleftharpoons NH_4^+ + DN^-$	2.90×10^{13}	-0.24	4349
8	$ADN_I \rightleftharpoons NH_3 + HDN_I$	2.21×10^{13}	-0.01	15737
9	$ADN_{IIa} \rightleftharpoons NH_3 + HDN_{IIa}$	5.95×10^{13}	-0.24	23189
10	$ADN_{IIb} \rightleftharpoons NH_3 + HDN_{IIb}$	1.84×10^{14}	-0.24	20051
11	$ADN_{IIc} \rightleftharpoons NH_3 + HDN_{IIc}$	6.10×10^{15}	-0.24	27302
12	$ADN_I \rightleftharpoons AN + N_2O$	2.03×10^{11}	0.31	45903
13	$ADN_{IIa} \rightleftharpoons AN + N_2O$	5.48×10^{13}	0.39	47298
14	$ADN_{IIb} \rightleftharpoons AN + N_2O$	4.79×10^{13}	0.28	43791
15	$ADN_{IIc} \rightleftharpoons AN + N_2O$	1.97×10^{13}	0.44	46048
16	$ADN_{IId} \rightleftharpoons AN + N_2O$	1.76×10^{13}	0.46	49351

17	$NH_4^+ + DN^- \rightleftharpoons AN + N_2O$	1.54×10^2	3.40	36959
18	$ADN_I \rightarrow \ NH_4NNO_2\cdot + NO_2\cdot$	1.48×10^{15}	-0.03	39910
19	$NH_4NNO_2\cdot + NO_2\cdot \rightarrow ADN_I$	1.00×10^{12}	0	0
20	$ADN_{IIa} \rightarrow \ NNO_2NH_4\cdot + NO_2\cdot$	5.43×10^{13}	0.42	36223
21	$NNO_2NH_4\cdot + NO_2\cdot \rightarrow ADN_{IIa}$	1.00×10^{12}	0	0
22	$ADN_{IIb} \rightarrow \ NNO_2NH_4\cdot + NO_2\cdot$	1.02×10^{14}	0.28	33981
23	$NNO_2NH_4\cdot + NO_2\cdot \rightarrow ADN_{IIb}$	1.00×10^{12}	0	0
24	$ADN_{IIc} \rightarrow \ NNO_2NH_4\cdot + NO_2\cdot$	9.82×10^{15}	-0.34	33975
25	$NNO_2NH_4\cdot + NO_2\cdot \rightarrow ADN_{IIc}$	1.00×10^{12}	0	0
26	$ADN_{IId} \rightarrow \ NNO_2NH_4\cdot + NO_2\cdot$	5.85×10^{11}	1.07	35324
27	$NNO_2NH_4\cdot + NO_2\cdot \rightarrow ADN_{IId}$	1.00×10^{12}	0	0
28	$NH_4NNO_2\cdot \rightleftharpoons NNO_2NH_4\cdot$	3.36×10^{11}	0.01	-60
29	$NNO_2NH_4\cdot \rightleftharpoons N_2O + NH_3 + OH\cdot$	2.27×10^{10}	0.78	12828
30	$NNO_2^-\cdot + NH_4^+ \rightleftharpoons NH_4NNO_2\cdot$	1.00×10^{12}	0	0
31	$NNO_2^-\cdot + NH_4^+ \rightleftharpoons NNO_2NH_4\cdot$	1.00×10^{12}	0	0
32	$HNNO_2\cdot + NH_3 \rightleftharpoons NH_4NNO_2\cdot$	1.00×10^{12}	0	0
33	$NNO_2H\cdot + NH_3 \rightleftharpoons NNO_2NH_4\cdot$	1.00×10^{12}	0	0
34	$HDN_I \rightleftharpoons HDN_{IIa}$	2.47	3.44	25748
35	$HDN_{IIa} \rightleftharpoons HDN_{IIb}$	5.20×10^{12}	0.10	3332
36	$HDN_{IIb} \rightleftharpoons HDN_{IIc}$	6.79×10^{11}	0.07	20683
37	$HDN_{IIc} \rightleftharpoons HDN_{IId}$	3.36×10^{10}	1.08	4735
39	$HDN_{IId} \rightleftharpoons HDN_{IIa}$	4.33×10^{10}	0.06	19141
39	$HDN_I + HDN_I \rightleftharpoons HDN_{IIa} + HDN_{IIa}$	2.34×10^{-3}	3.56	5885
40	$HDN_{IIb} + HDN_{IIb} \rightleftharpoons HDN_{IIc} + HDN_{IIc}$	5.16×10^{-3}	3.61	-2098
41	$HDN_I \rightleftharpoons HNO_3 + N_2O$	1.35×10^{12}	0.33	36500
42	$HDN_{IIa} \rightleftharpoons HNO_3 + N_2O$	1.07×10^{12}	0.34	36681
43	$HDN_{IIb} \rightleftharpoons HNO_3 + N_2O$	1.24×10^{12}	0.38	35652
44	$HDN_{IIc} \rightleftharpoons HNO_3 + N_2O$	9.07×10^9	1.69	38416
45	$HDN_I + NO_3^- \rightleftharpoons DN^- + HNO_3$	1.00×10^{12}	0	0
46	$HDN_{IIa} + NO_3^- \rightleftharpoons DN^- + HNO_3$	1.00×10^{12}	0	0
47	$HDN_{IIb} + NO_3^- \rightleftharpoons DN^- + HNO_3$	1.00×10^{12}	0	0
48	$HDN_{IIc} + NO_3^- \rightleftharpoons DN^- + HNO_3$	1.00×10^{12}	0	0
49	$HDN_{IId} + NO_3^- \rightleftharpoons DN^- + HNO_3$	1.00×10^{12}	0	0
50	$HDN_I \rightleftharpoons HNNO_2 + NO_2\cdot$	398×10^{13}	0.08	36013
51	$HDN_{IIa} \rightleftharpoons NNO_2H + NO_2\cdot$	1.19×10^{12}	1.23	31147

52	$HDN_{IIb} \rightleftharpoons NNO_2H + NO_2\cdot$	3.22×10^{24}	-2.55	37480
53	$HDN_{IIc} \rightleftharpoons NNO_2H + NO_2\cdot$	7.31×10^{13}	1.07	31205
54	$HDN_{IId} \rightleftharpoons NNO_2H + NO_2\cdot$	1.34×10^{14}	0.34	31525
55	$HNNO_2\cdot \rightleftharpoons NNO_2H\cdot$	3.61×10^{-1}	3.68	20628
56	$HNNO_2\cdot + H_2O \rightleftharpoons NNO_2H + H_2O$	4.15×10^{1}	2.80	10005
57	$NNO_2H\cdot \rightleftharpoons N_2O + OH\cdot$	3.88×10^{12}	0.43	3996
58	$HNNO_2 + NO_2\cdot \rightleftharpoons ONONHNO_2$	4.38	2.89	1120
59	$ONONHNO_2 \rightleftharpoons NH(O)NO_2\cdot + NO\cdot$	3.91×10^{13}	-0.06	5864
60	$NH(O)NO_2\cdot \rightleftharpoons HNO + NO_2\cdot$	6.65×10^{13}	0.30	4095
61	$NNO_2H\cdot + NO_2\cdot \rightleftharpoons ONONN(OH)O$	8.55	2.99	-5374
62	$ONONN(OH)O \rightleftharpoons ONNO + HONO$	3.42×10^{12}	0.37	22261
63	$ONONN(OH)O \rightleftharpoons NO\cdot + ONNO_2H\cdot$	1.64×10^{13}	0.28	14412
64	$ONNO_2H\cdot \rightleftharpoons HONO + NO\cdot$	1.35×10^{13}	-0.02	364
70	$DN^- \rightleftharpoons NO_3^- + N_2O$	1.07×10^{12}	1.29	46994
71	$DN^- \rightarrow NNO_2^-\cdot + NO_2\cdot$	6.86×10^{14}	-0.09	41309
73	$NNO_2^-\cdot + NO_2 \rightleftharpoons ONONNO_2^-$	1.25×10^{1}	3.12	1720
74	$ONONNO_2^- \rightleftharpoons ONNO + NO_2^-$	1.41×10^{12}	0.24	17862
75	$ONNO + NO_2^- \rightleftharpoons NO_3^- + N_2O$	5.75×10^{1}	2.85	-2643
76	$ONNO \rightleftharpoons NO\cdot + NO\cdot$	6.20×10^{12}	0.22	6679
77	$NNO_2^- + t\text{-}ONONO_2 \rightleftharpoons NO_3^- + N_2O + NO_2$	6.70	3.07	706
78	$NNO_2^-\cdot + NO \rightleftharpoons ONNNO_2^-$	3.89×10^{3}	2.48	-1780
79	$ONNNO_2^- \rightleftharpoons NO_2^- + N_2O$	7.44×10^{12}	0.29	20452

2.2 Thermodynamic data

Thermodynamic data were developed based on quantum chemistry calculations using the

Gaussian 09 program package [34]. Optimization and frequency analysis were conducted

using the G4 [35] and the G4/SCRF = (solvent = water) level of theory. Solvent effects were

included by application of the self-consistent reaction field (SCRF) and polarizable

continuum model (PCM) options within the program when investigating the liquid species in

molten ADN. However, no solvent parameters of molten ADN were available; therefore,

water solvation was used to determine the solvent effect when examining reactions in molten

ADN. The dielectric constant (the e value of water is 78.3553) is one of the important

parameters involved in the solvation effect. The dielectric constants (e) of ammonium-based

protic ionic-liquids are substantially higher than those of aprotic ionic-liquids. The dielectric

11

constants of ethylammonium nitrate and methylammonium formate are 26.2 and 41.0,

respectively [36]. Dielectric constants tend to increase with increasing length of the alkyl

chain. Thus, we have believed that molten ammonium salts including ADN have a large value

of e. Yamashita and Asai [37] measured e for ammonium nitrate (AN), which is typical

ammonium-based protic salt that is analogous with ADN. AN is also a major product from the

decomposition of ADN. The dielectric constant for AN has been reported to be approximately

40 at 383 K, and it is also reported that the dielectric constant tends to increase with the

temperature [37]. In addition to this, novel ADN-based monopropellants LMP-103S and

FLP-106, which are novel ADN-based monopropellants invented and tested within a

co-operative project between the Swedish Space Corporation and the Swedish Defense

Research Agency, are a blend of ADN, water, methanol, and ammonia [1]. Water solvation

effects can provide some insights into chemical reactions in such ADN-based propellants.

Although we have used the water solvation effect as a substitute for liquid ADN in this study,

the water solvation effect should be replaced with a more adequate solvation effect in future

work.

Thermal correction, entropy (S_{liq}), and heat capacity (C_P) values were calculated from the

partition function using statistical mechanics, employing the GPOP software [31]. The heats

of formation for gas-phase molecules ($\Delta_f H_{gas}^{\circ}$) were calculated by the traditional atomization

12

method (ARM-1) [38]. The standard heat of formation for a compound in solution is obtained

from the gas-phase heat of formation and the enthalpy of solvation at 298.15 K, as in the

following two equations.

$$\Delta_f H^\circ_{\text{liq}} = \Delta_f H^\circ_{\text{gas}} + \Delta_{solv} H^\circ \tag{2}$$

$$\Delta_{\text{solv}} H^\circ = H_{\text{liq, calc}} - H_{\text{gas, calc}} \tag{3}$$

Here, $\Delta_{\text{solv}} H^\circ$ is the solvation enthalpy, and $H_{\text{liq, calc}}$ and $H_{\text{gas, calc}}$ are the heats of

formation at 298.15 K calculated directly using the G4 methods. Table 2 and 3 list the heats of

formation for gas and liquid phase compounds obtained from the G4 level of theory and

thermodynamic data.

In Table 2, the enthalpy of formation of 5 conformers of ADN in the liquid phase varies

from -43.6 to -47.6 kJ/mol. At the same time, the enthalpy of formation of ADN in solid phase

is -134.8 kJ mol^{-1} [39]. Considering the heat of solution (142 J mol^{-1} [1]), the enthalpy of

formation of ADN in the liquid phase can be calculated to be -134.7 kJ mol^{-1}. The calculated

value is much lower than ones obtained from this work. One of the possible reason is neglect

of larger cluster of ADN (bulk). An molecule in molten salt is surrounded by many other

molecules and larger clusters including several ADN units can exist in molten ADN. To obtain

precise the heat of formation of molten ADN, we should consider the large cluster of ADN.

This errors also result from the ideal gas treatment. In the quantum chemical calculation of

isolated systems, thermodynamic parameters are generally calculated by an ideal gas

treatment. The ideal gas treatment provides high performance for the evaluation of

thermodynamic parameters in gas phases. On the other hand, the calculation of

thermodynamic parameters in liquid phases with this continuum model involves unrealistic

results due to the overestimation of entropy factor.

Table 2. Calculated enthalpies (kJ mol^{-1}) for the formation of species associated with ADN decomposition. The estimated absolute value of 386.3 kJ mol^{-1} for $\Delta_f H°(H^+)$ [40].

	$\Delta_f H°_{gas,calc}$	$\Delta_{solv} H°_{calc}$	$\Delta_f H°_{aq,calc}$
ADN$_I$	18.3	-64.5	-46.2
ADN$_{IIa}$	21.6	-69.2	-47.6
ADN$_{IIb}$	19.4	-65.1	-45.7
ADN$_{IIc}$	26.3	-70.6	-44.3
ADN$_{IId}$	26.3	-69.8	-43.6
HDN$_I$	107.9	-21.8	86.1
HDN$_{IIa}$	123.80	-18.6	105.2
HDN$_{IIb}$	121.40	-19.4	102.0
HDN$_{IIc}$	130.6	-22.2	108.4
HDN$_{IId}$	124.0	-18.5	105.4
DN$^-$	-129.7	-217.2	39.3
NH$_4$NNO$_2$·	148.3	-46.8	101.5
NNO$_2$NH$_4$·	136.3	-49.9	86.4
HNNO$_2$·	222.1	-15.2	206.9
NNO$_2$H·	232.0	-14.0	218.0
NNO$_2$$^-$·	49.6	-246.0	189.9

14

ONONHNO$_2$	125.7	-18.8	106.9
ONONN(OH) O	163.0	-20.1	142.8
ONONNO$_2{}^-$	-23.8	-215.4	147.1
ONNO	247.7	-9.6	238.1

Table 3. Calculated thermodynamic data for species associated with ADN decomposition.

SPECIES	$\Delta_f H^{\circ}_{\text{liq,calc}}$	$S^{\circ}_{\text{liq,calc}}$	C_P [J K^{-1} mol^{-1}]						
	[kJ mol^{-1}]	[J mol^{-1} K^{-1}]	300	400	500	600	800	1000	1500 K
ADN$_I$	-46.2	414.42	130.27	151.33	169.76	185.26	208.75	225.19	249.44
ADN$_{IIa}$	-47.58	406.40	129.6	151.04	169.64	185.19	208.69	225.12	249.37
ADN$_{IIb}$	-45.68	410.41	129.92	151.25	169.79	185.33	208.81	225.22	249.44
ADN$_{IIc}$	-44.33	411.47	130.41	151.61	170.06	185.50	208.85	225.18	249.36
ADN$_{IId}$	-44.33	417.20	131.42	152.32	170.57	185.84	208.89	225.06	249.13
HDN$_I$	86.14	347.60	90.52	107.67	121.43	132.14	146.92	156.21	168.41
HDN$_{IIa}$	105.18	341.19	92.71	109.81	123.32	133.74	148.01	156.92	168.64
HDN$_{IIb}$	102.04	344.91	93.02	109.92	123.32	133.68	147.91	156.82	168.57
HDN$_{IIc}$	108.39	343.65	93.79	110.69	123.95	134.18	148.22	157.02	168.65
HDN$_{IId}$	105.44	326.58	87.08	105.56	120.29	131.74	147.58	157.45	169.89
DN$^-$	39.33	325.33	83.88	99.61	112.14	121.67	134.25	141.56	150.05
NH$_4$NNO$_2\cdot$	101.48	332.62	83.96	97.77	110.43	121.50	138.99	151.74	171.33
NNO$_2$NH$_4\cdot$	86.38	348.79	92.99	106.76	119.30	130.24	147.53	160.18	179.67
HNNO$_2\cdot$	206.89	289.37	58.10	66.40	73.21	78.63	86.35	91.46	98.66
NNO$_2$H$\cdot$	218.01	276.08	57.33	66.29	73.35	78.81	86.39	91.32	98.33
NNO$_2{}^-\cdot$	189.94	267.54	47.47	55.13	61.27	65.92	71.99	75.48	79.47

ONONHNO$_2$	106.90	350.07	98.82	114.28	126.44	135.91	149.16	157.66	169.06
ONONNO$_2$H	142.88	345.92	101.97	117.81	129.77	138.83	151.23	159.07	169.61
ONONNO$_2{}^-$	106.40	339.18	91.18	106.02	117.35	125.82	136.93	143.40	150.92

2.3 Detailed chemical reaction simulation

The YNU-L 2.0 model was developed in the present work, which consists of various kinetic

parameters (a total of 138 reactions) and the thermodynamic data (for 57 species) shown in

Tables 1 and 3. To better understand the decomposition process for ADN, the YNU-L 2.0

mechanism was employed to predict the decomposition of ADN in an adiabatic reactor at

constant enthalpy and volume. These calculations were performed with the CHEMKIN-PRO

software package [41]. The associated CHEMKIN-format model (based on the relevant

kinetic and thermodynamic data) is provided in the Supporting Information. The initial

density was set to 1.675 g cm^{-3}, which is the density of pure liquid ADN [1], and the

16

decomposition reactions were simulated at a heating rate of 5 K min^{-1} (a typical heating rate

in thermal analysis) from 363 to 623 K.

3. Experimental

Differential scanning calorimetry (DSC; TA instruments Q200) was used to examine the

thermal behavior of ADN and to validate the YNU-L 2.0 model. The DSC apparatus was

calibrated for temperature and heat flow by the melting of high-purity indium (99.99%) at a

scanning rate of 5 K/min. Samples of approximately 1.0 mg were placed in stainless steel

pans under atmospheric air pressure at 0.1 MPa. Each pan was sealed with a stainless steel lid.

The samples were heated from 303 to 623 K at a rate of 5 K min^{-1}.

4. Results and discussion

To validate the YNU-L2.0 model, the simulated heat flow curve was compared with the DSC

result for the sealed condition. Figure 2 shows heat flow curves obtained from simulation

based on the YNU-L2.0 model and experimental DSC measurements at a heating rate of 5 K

min[-1]. Many DSC measurements have been applied to study physicochemical properties and

thermal decomposition [15,16]. A typical DSC curve for ADN under open atmospheric

conditions exhibits thermal events such as a melting endotherm (366 K), decomposition

17

exotherm, and sublimation endotherm. The onset of thermal decomposition is at $T_{\text{decomp.}} \approx$ 423–428 K and the exothermic peak is observed around $T_{\text{exo.}} \approx$ 443–448 K [15,16]. Under the sealed condition, ADN showed a doublet decomposition peak with an additional exothermic peak at 583 K [15,16,20,21,23]. Two peaks are caused by the exothermal decomposition of ADN (the first peak) and that of AN formed during ADN decomposition (the second peak) [16]. Both of the heat flow curves for ADN showed a doublet decomposition peak as reported in the literature [15,16,20,21,23]. The simulated onset of thermal decomposition is at $T_{\text{decomp., sim.}}$ = 423 K, based on the intersection of the tangents of the peak with the extrapolated baseline, and the exothermic peak is observed around $T_{\text{exo., sim.}}$ = 450 K. These values are in good agreement with the DSC results ($T_{\text{decomp., DSC}}$ = 425 K, $T_{\text{exo., DSC}}$ = 453 K) and those values reported in the literature [16]. The heat of reaction for the first peak was calculated to be 1.9 kJ g^{-1} in this simulation, which was in good agreement with that in the literature. The heat of decomposition obtained from DSC measurements has been reported to be 1.93±0.32 [16], 1.8 [18], and 1.85-2.02 kJ g^{-1} [20]. The simulated profile and thermal properties are excellently match the experimental DSC measurements.
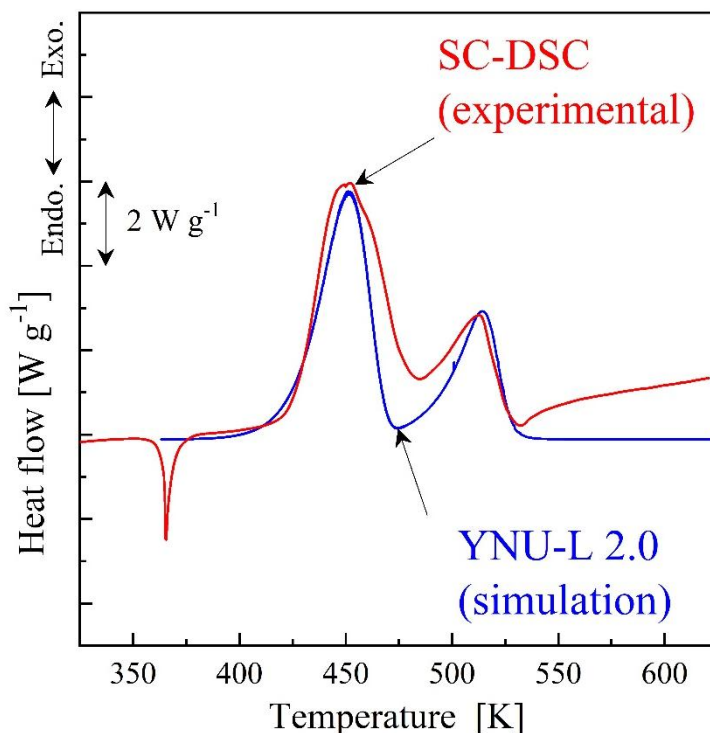
Figure 2. Heat flow curves obtained from DSC measurements and simulation with the YNU-L2.0 model.

The simulated temperature-change profiles of various species at a heating rate of 5 K min^{-1} are shown in Figure 3. At 363 K, the ion-pair complex ADNs, the dissociated ions (NH$_4^+$ and DN$^-$), and a minor amount of the base and acid forms (HDN and NH$_3$) are all present in chemical equilibrium in molten ADN. The sum of the moles of ADNs, DN$^-$, and HDNs, which indicate the unreacted moles of ADN, is plotted in Figure 3. This value begins to decrease at approximately 423 K, which is the onset temperature of the exothermic reaction.

The Kissinger method was employed to elaborate the concentration change curve at heating

rate of 2.5, 5, 10 and 20 K min^{-1} from detailed reaction simulations based on the YNU-L2.0

model. The details on kinetic analysis and its results are shown in supporting information. The

apparent activation energy and frequency factor were calculated to be 145.3 kJ mol^{-1} and 1.69

$\times$ 10^{14} s^{-1}, respectively. This rate constant agree with previous works by Russian groups

$(1.46 \times 10^{16}$ exp(-161000 R^{-1} T^{-1}) [42] and 2.5×10^{14} exp(-148000 R^{-1} T^{-1}) [43]). The

proposed kinetics model can provide the kinetics of the limiting reaction during

decomposition and combustion.

Figure 3 also reveals that the moles of the major products of H_2O, N_2O, N_2, and AN begin

to increase at the onset temperature of 423 K, and then the moles of AN decrease and the

moles of N_2O and H_2O increase again at above approximately 473 K. Decomposition gases

from ADN were well investigated using Fourier transform-infrared spectroscopy (FT-IR) and

mass spectrometry (MS) measurements [24]; the main products of decomposition at a heating

rate of 5 K min^{-1} were AN, H_2O, and N_2O, and the minor product was N_2. This new model

therefore predicts the same evolved gases as those reported in previous studies.
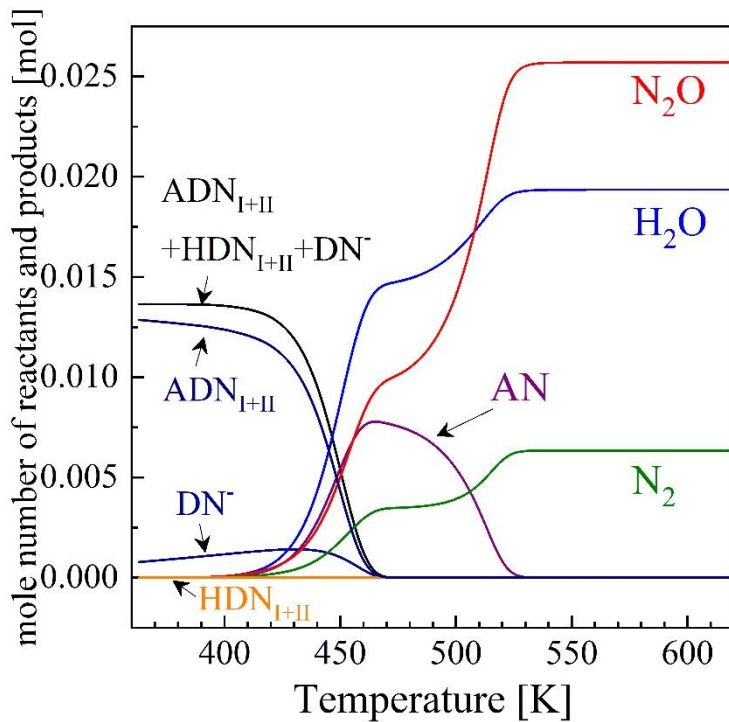
Figure 3. Variations in the ADN decomposition species over time at a heating rate of 5 K min^{-1}.

Another validation study was conducted to compare the chemical composition changes in the liquid phase. Matsunaga et al. [30] conducted DSC measurements combined with Raman spectroscopy (DSC-Raman) to elucidate the composition changes in the liquid phase during thermal decomposition. Figure 4 shows the change of the molar ratio of ADN and AN in the liquid phase as a function of temperature. From approximately 413 K, the amount of ADN began to decrease, while the amount of AN began to increase. The solid lines in Figure 4 show the changes in the concentrations of ADN and AN with the temperature simulated based

on the YNU-L2.0 model. The trend of the simulation lines show an excellent match with the experimental plots for the molar ratio of ADN and AN at below approximately 442 K. Above 442 K, the difference between the simulated lines and the experimental plots is larger. This difference is caused by omitting physical changes. The thermal behavior of ADN decomposition under open atmospheric conditions is affected by the thermal behavior of AN because the temperature above 442 K is the melting point of AN and melted AN begins to undergo endothermic sublimation. The DSC-Raman study reported by Matsunaga et al. [30] was conducted under open atmospheric conditions. Therefore, the concentration profiles of AN and ADN were affected by the endothermic sublimation of AN, and the YNU-L2.0 model without physical changes (AN sublimation) could not match the experimental data under atmospheric conditions above 442 K.

From the two validation studies, it was concluded that the YNU-L 2.0 model has been validated and can provide good predictions of the liquid-phase decomposition of ADN. Despite such good predictions, the model should be improved with respect to various points. In future work, the new model should include physical changes to improve the simulation of ADN decomposition, and it should use more suitable solvation effects to obtain accurate thermodynamic data.
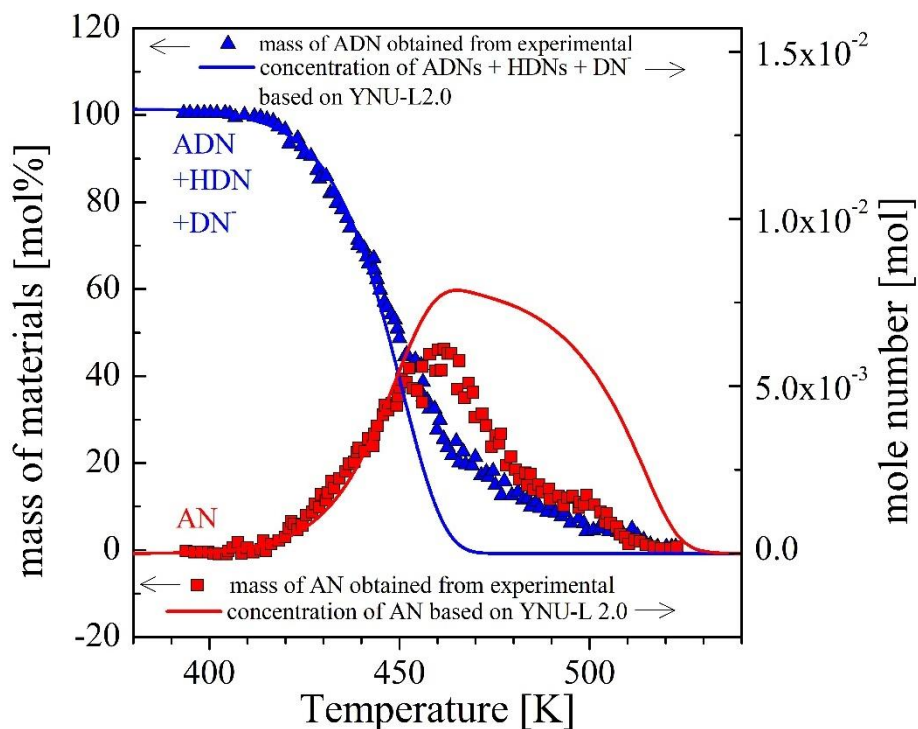
Figure 4 Variations of ADN and AN in the condensed phase over time at a heating rate of 5

K min^{-1}. Experimental DSC-Raman measurements from Ref. [30] and simulated data based

on the YNU-L 2.0 model are plotted.

A possible decomposition mechanism has been elucidated from the rate of production

(ROP) based on the YNU-L2.0 model. Figure 5 shows the ROP results for important species

(NO$_2$·, and OH·) during the first exothermic decomposition. The ROP data indicate those

elemental reactions that play important roles in the production or reduction of a species.

Figure 5a shows that NO$_2$· decreases via the reaction ADN$_{II}$ (ADN$_{IIb}$ and ADN$_{IIc}$ in Figure 1)

→ NO$_2$· + NNO$_2$NH$_4$·. The dissociated NO$_2$ combines with OH· to yield HNO$_3$, or binds with

other NH_2 to form NH_2NO_2 or NH_2ONO.

Figure 5b summarizes the ROP data for $OH\cdot$. Following the decomposition of ADN_{II}, the resultant NNO_2NH_4 decomposes to produce $OH\cdot$, NH_3, and N_2O. The major part of produced $OH\cdot$ immediately recombines with $NO_2\cdot$ from ADN_{II} to yield HNO_3, or a minor part of the $OH\cdot$ attacks NH_3 to produce $NH_2\cdot$ and H_2O. After the former path, the HNO_3 bonds to NH_3 to yield AN as a stable intermediate. The major reaction scheme for ADN can be written as follows.

$ADN_{II} \rightarrow NNO_2NH_4\cdot + NO_2\cdot$

$NNO_2NH_4\cdot \rightarrow NH_3 + N_2O + OH\cdot$

$NO_2\cdot + OH\cdot \rightarrow HNO_3$

$NH_3 + HNO_3 \rightarrow NH_4NO_3$

(overall) $ADN_{II} \rightarrow N_2O + NH_4NO_3$
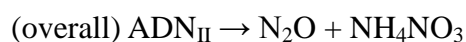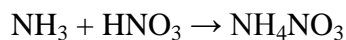
In the minor path, NH_2 bonds to $NO_2\cdot$ to yield NH_2NO_2 (nitramide) or NH_2ONO. NH_2NO_2 decomposes to N_2O and H_2O via the isomer $NHNO_2H$ [25]. NH_2ONO decomposes to $NH_2O\cdot$ and $NO\cdot$ via homolytic cleavage of the NH_2O-NO bond. After the bonding of $NO\cdot$ and $NH_2\cdot$, the resultant NH_2NO decomposes to produce N_2 and H_2O via $NHNOH$. $NH_2O\cdot$ is attacked by $NO_2\cdot$ to form $HONO$ and HNO. $HONO$ decomposes with HNO_3 to yield two $NO_2\cdot$ via *trans*-$ONONO_2$, and HNO reacts with $NO_2\cdot$ to yield $NO\cdot$ and $HONO$. HNO also dimerizes

24

and decomposes to yield N_2O and H_2O [44]. The second exothermic decomposition (AN

decomposition) was investigated in our previous study [45]. Figure 6 shows a schematic

diagram of decomposition of ADN. In general, the decomposition of major energetic salt

begins with an acid-base dissociation, after which the acidic species decomposes or attacks

the base. ADN is thought to decompose via this same mechanism [15, 16, 21]. Including the

acid-base dissociation (ADN $\rightarrow$ HDN + NH_3), the YNU-L2.0 model contains possible

reaction paths reported in the previous studies [8, 15, 16, 21, 46]. However, the detailed

kinetic model revealed that molten ADN appears to directly decompose without acid-base

dissociation.
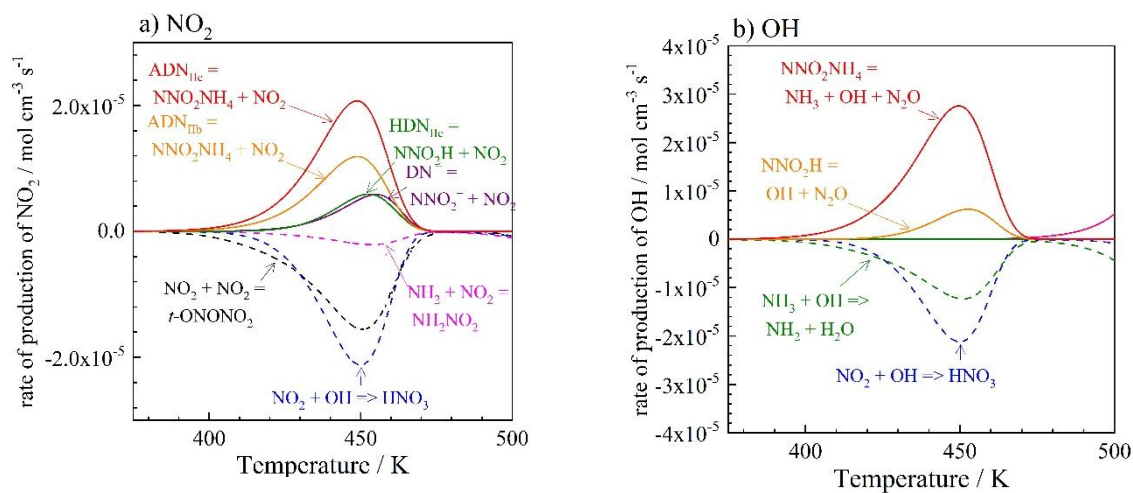
Figure 5. ROP data for important species during ADN decomposition: a) $NO_2\cdot$ and b) $OH\cdot$
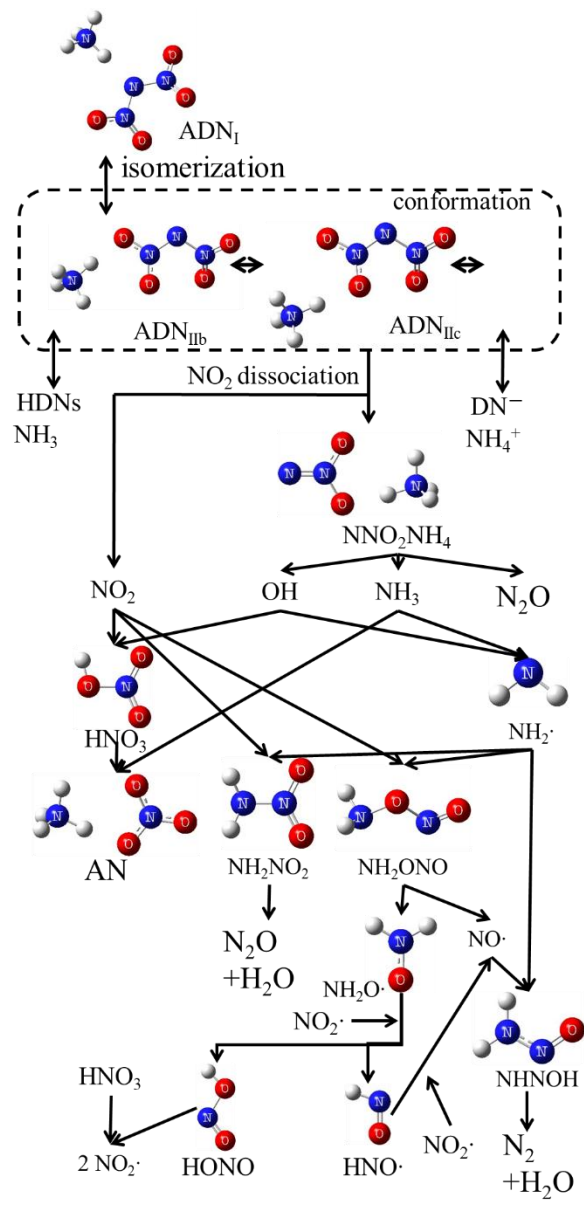
Figure 6. Decomposition pathways for liquid ADN.

5. Conclusions

A detailed chemical kinetic model (YNU-L 2.0) was developed for ADN decomposition in the liquid phase. Rate coefficients were calculated to perform TST and VTST analyses of the reactions identified in a previous study [27]. The rate coefficients for radical recombination reactions and proton transfer with no energy barriers were set to the diffusion limited value of 10^{12} cm^3 mol^{-1} s^{-1}. Thermal correction, entropy, and heat capacity values were then calculated from the partition function using statistical mechanics. The heats of formation for gas and liquid phase molecules were determined by the traditional atomization method combined with the G4 and G4/SCRF=(PCM, solvent=water) level of theory.

The YNU-L 2.0 model consists of 118 reactions and 78 species, and the model successfully predicts the thermal decomposition of ADN at a heating rate of 5 K min^{-1}. The predicted thermal properties ($T_{\text{decomp., sim.}}$ = 423 K, $T_{\text{exo., sim.}}$ = 450 K, $Q_{\text{exo., sim.}}$ = 1.9 kJ mol^{-1}) are in good agreement with the experimental properties ($T_{\text{decomp., DSC}}$ = 425 K, $T_{\text{exo., DSC}}$ = 453 K, $Q_{\text{exo., DSC}}$ = 1.8–2.0 kJ mol^{-1}). The new model can also simulate a species change in the condensed phase, and the predicted molar changes of ADN and AN were an excellent match with the experimentally observed changes obtained from DSC-Raman measurements. The model also calculated the evolved gases, and the gases were reasonable compared with the evolved gases detected experimentally using TG-DTA-MS. Therefore, it was concluded that the YNU-L 2.0 model has been validated. In future work, the model should include physical changes and use

27

more suitable solvation effects.

The YNU-L 2.0 model has revealed the detailed decomposition mechanism based on first principles. The initial reaction $ADN_{II} \rightarrow NNO_2NH_4 + NO_2$ triggers the overall decomposition, and subsequent $NNO_2NH_4 \cdot \rightarrow NNO_2H \cdot + NH_3$, $NNO_2H \cdot \rightarrow N_2O + OH \cdot$, $NO_2 \cdot + OH \cdot \rightarrow HNO_3$, and $NH_3 + HNO_3 \rightarrow NH_4NO_3$ consist of a well-known one-step formula: $ADN \rightarrow N_2O + NH_4NO_3$. A minor part of $OH \cdot$ attacks NH_3, and the subsequent radical reaction path yields N_2 and H_2O.

In the future, our model should be improved in various aspects. For example, our model needs more experimental validations, and the reduction of detailed chemical kinetic mechanisms is needed for engineering utilization. We are also seeking for not only a precise but also theoretically-supported solvation-model to evaluate the entropy of species in ionic solutions.

28

6. References

[1] A. Larsson, N. Wingborg, Green propellants based on ammonium dinitramide, in: J. Hall (Ed.), Advances in Spacecraft Technologies, InTech, Rijeka, HR., 2011, pp. 139-156.

[2] M.Y. Nagamachi, J.I. Oliveira, A.M. Kawamoto, R.C.L. Dutra, ADN - The new oxidizer around the corner for an environmentally friendly smokeless propellant, J. Aeros. Technol. Manage. 153 (2009) 153-160.

[3] H. Östmark, U. Bemm, A. Langlet, R. Sanden, N. Wingborg, The properties of ammonium dinitramide (ADN): Part 1, basic properties and spectroscopic data, J. Energ. Mater. 18 (2000) 123-138.

[4] P. Thakre, Y. Duan, V. Yang, Modeling of ammonium dinitramide (ADN) monopropellant combustion with coupled condensed and gas phase kinetics, Combust. Flame 161 (2014) 347-362.

[5] V.P. Sinditskii, V.Y. Egorshev, A.I. Levshenkov, V.V. Serushkin, Ammonium nitrate: Combustion mechanism and the role of additives, Propellant Explos. Pyrotech. 30 (2005) 269-280.

[6] V.P. Sinditskii, V.Y. Egorshev, V.V. Serushkin, S.A. Filatov, Combustion of energetic materials controlled by condensed-phase reactions, Combust. Explos. Shock Waves 48 (2012) 81-99.

29

[7] N.E. Ermolin, Modeling of pyrolysis of ammonium dinitramide sublimatin products under low-pressure conditions, Combust. Explos. Shock Waves 40 (2004) 92-106.

[8] J. Park, D. Chakraborty, M.C. Lin, Thermal decomposition of gaseous ammonium dinitramide at low pressure: Kinetic modeling of product formation with ab initio MO/cVRRKM calculations, Symp. (int.) Combust. 27 (1998) 2351-2357.

[9] Y. Izato, M. Koshi, A. Miyake, A detailed chemical kinetics model for the initial decomposition of gas-phase hydroxylamine, Sci. Technol. Energetic Materials 78 (2017) 12-18.

[10] S. Raman, R.W. Ashcraft, M. Vial, M.L. Klasky, Oxidation of hydroxylamine by nitrous and nitric acids. Model development from first principle SCRF calculations, J. Phys. Chem. A 109 (2005) 8526-8536.

[11] R.W. Ashcraft, S. Raman, W.H. Green, Ab initio aqueous thermochemistry: application to the oxidation of hydroxylamine in nitric acid solution, J. Phys. Chem. B 111 (2007) 11968-11983.

[12] R.W. Ashcraft, S. Raman, W.H. Green, Predicted reaction rates of $H_xN_yO_z$ intermediates in the oxidation of hydroxylamine by aqueous nitric acid, J. Phys. Chem. A 112 (2008) 7577-7593.

[13] N.R. Kumbhakarna, K.J. Shah, A. Chowdhury, S. T. Thynell, Thermochim. Acta 590

(2014) 51-65.

[14] N. Kumbhakarna, S.T. Thynell, Development of a reaction mechanism for liquid-phase decomposition of guanidinium 5-amino tetrazolate, Thermochim. Acta 582 (2014) 25-34.

[15] R. Yang, P. Thakre, V. Yang, Thermal decomposition and combustion of ammonium dinitramide, Combust. Explos. Shock Waves 41 (2005) 657-679.

[16] N.E. Ermolin, V.M. Fomin, On the mechanism of thermal decomposition of ammonium dinitramide, Combust. Explos. Shock Waves 52 (2016) 556-586.

[17] A. Langlet, N. Wingborg, H. Östmart, ADN: A new high performance oxidizer for solid propellants, in: K. Kuo (Ed.) Challenges in Propellants and Combustion: 100 Years after Nobel, Begell House, Danbury, Connecticut; 1997, pp. 616-626.

[18] H. Matsunaga, H. Habu, A. Miyake, Thermal decomposition of the high-performance oxidizer ammonium dinitramide under pressure, J. Therm. Anal. Calorim. 116 (2014) 1227-1232.

[19] H. Matsunaga, Y. Izato, H. Habu, A. Miyake, Thermal decomposition characteristics of mixtures of ammonium dinitramide and copper (II) oxide, J. Therm. Anal. Calorim. 121 (2015) 319-326.

[20] A.S. Tompa, Thermal analysis of ammonium dinitramide (ADN), Thermochim. Acta 357-358 (1999) 177-193.

[21] J.C. Oxley, J.L. Smith, W. Zhang, Thermal decomposition studies on ammonium dinitramide (ADN) and ^{15}N and ^{2}H isotopomers, J. Phys. Chem. 101 (1997) 5646-5652.

[22] S. Vyazovkin, C. Wight, Isothermal and nonisothermal reaction kinetics in solids: in search of ways toward consensus, J. Phys. Chem. 101 (1997) 5653-5658.

[23] H. Matsunaga, H. Habu, A. Miyake, Thermal behavior of new oxidizer ammonium dinitramide, J. Therm. Anal. Calorim. 111 (2013) 1183-1188.

[24] Y. Izato, H. Habu, M. Koshi, A. Miyake, Kinetics analysis of thermal decomposition of ammonium dinitramide (ADN), J. Therm. Anal. Calorim. 127 (2016) 255-264.

[25] Y. Izato, M. Koshi, A. Miyake, Identification of thermal decomposition products and reactions for liquid ammonium nitrate on the basis of ab initio calculation, Int. J. Chem. Kinet. 49 (2016) 83-99.

[26] N.V. Muravyev, N. Koga, D.B. Meerov, A.N. Pivkina, Kinetic analysis of overlapping multistep thermal decomposition comprising exothermic and endothermic processes: thermolysis of ammonium dinitramide, Phys. Chem. Chem. Phys. 19 (2017) 3254-3264.

[27] Y. Izato, A. Miyake, The decomposition pathways of ammonium dinitramide on the basis of ab initio calculations, J. Energ. Mater. (2017), doi.org/10.1080/07370652.2017.1405099.

[28] J.A. Montgomery, M. J. Frisch, J. W. Ochterski, G. A. Petersson, A complete basis set model chemistry. VI. Use of density functional geometries and frequencies, J. Chem. Phys.

110 (1999) 2822-2827.

[29] J. D. Chai, M. Head-Gordon, Long-range corrected hybrid density functionals with damped atom–atom dispersion corrections, Phys. Chem. Chem. Phys. 10 (2008) 6615-6620.

[30] H. Matsunaga, H. Habu, A. Miyake, Analysis of thermal decomposition behavior of high-energy solid propellant oxidizer ammonium dinitramide, Proc' Int. Symp. Space Technol. Sci., 29th (2013), paper 2013-a-17.

[31] A. Miyoshi, GPOP software, rev. 2013.07.15m7, available from the author. See http://akrmys.com/gpop/. (Accessed 18 June 2018).

[32] J. I. Steinfeld, J. S. Francisco, W. L. Hase, Chemical Kinetics and Dynamics, 2nd ed.; Prentice Hall, Upper Saddle River, N.J., 1998.

[33] M. Rahm, T. Brinck, On the Anomalous decomposition and reactivity of ammonium and potassium dinitramide. J. Phys. Chem. A 114 (2010) 2845-2854.

[34] M. J. Frisch, G.W. Trucks, H.B. Schlegel, G.E. Scuseria, M.A. Robb, J.R. Cheeseman, G. Scalmani, V. Barone, B. Mennucci, G. A. Petersson, H. Nakatsuji, M. Caricato, X. Li, H.P. Hratchian, A.F. Izmaylov, J. Bloino, G. Zheng, J.L. Sonnenberg, M. Hada, M. Ehara, K. Toyota, R. Fukuda, J. Hasegawa, M. Ishida, T. Nakajima, Y. Honda, O. Kitao, H. Nakai, T. Vreven, J.A. Montgomery, J.E. Peralta, F. Ogliaro, M. Bearpark, J.J. Heyd, E. Brothers, K.N. Kudin, V.N. Staroverov, T. Keith, R. Kobayashi, J. Normand, K. Raghavachari, A. Rendell, J.

C. Burant, S.S. Iyengar, J. Tomasi, M. Cossi, N. Rega, J.M. Millam, M. Klene, J.E. Knox, J.B. Cross, V. Bakken, C. Adamo, J. Jaramillo, R. Gomperts, R.E. Stratmann, O. Yazyev, A.J. Austin, R. Cammi, C. Pomelli, J.W. Ochterski, R.L. Martin, K. Morokuma, V.G. Zakrzewski, G.A. Voth, P. Salvador, J.J. Dannenberg, S. Dapprich, A.D. Daniels, O. Farkas, J.B. Foresman, J.V. Ortiz, J. Cioslowski, D.J. Fox, Gaussian 09, Revision D.01, Gaussian, Inc., Wallingford CT (2010)

[35] L. A. Curtiss, P. C. Redfern, K. Raghavachari, Gaussian-4 theory, J. Chem. Phys. 126 (2007) 1-12.

[36] M. Huang, Y. Jiang, P. Sasisanker, G. W. Driver, H. Weingärtner, Static relative dielectric permittivities of ionic liquids at 25 C, J. Chem. Eng. Data 56 (2011) 1494-1499.

[37] A. Yamashita, K. Asai, Dielectric anomaly of ammonium nitrate in low frequency region, J. Phys. Soc. Japan 18 (1963) 1247-1253.

[38] J. W. Ochterski, Thermochemistry in gaussian, Gaussian, Inc., Wallingford CT (2000), http://www.lct.jussieu.fr/manuels/Gaussian03/g_whitepap/thermo/thermo.pdf.

[39] T. S. Kon'kova, Y. N. Matyushin, E. A. Miroshnichenko, and A. B. Russ. Chem. Bull. 58 (2009) 2020-2027.

[40] T. R. Tuttle, S. Malaxos, J. V. J. Coe, A new cluster pair method of determining absolute single ion solvation energies demonstrated in water and applied to ammonia, J. Phys. Chem. A

106 (2002) 925-932.

[41] CHEMKIN PRO: a chemical kinetics package for the analysis of gas-phase chemical

kinetics, Reaction Design, 2008.

[42] V. P. Sinditskii, V. Y. Egorshev, A. I. Levshenkov, and V. V. Serushkin, Combustion of

ammonium dinitramide, part 2: combustion mechanism, J. Propul. Power 22 (2006) 777-785.

[43] G. B. Manelis, G. M. Nazin, Y. I. Rubtsov, and V. A. Strunin, Thermal decomposition and

combustion of explosives and propellants, Taylor and Francis, New York, U.S.A., 2003. pp.

221-231.

[44] K. Zhang, S. Thynell, Examination of the mechanism of the yield of N_2O from nitroxyl

(HNO) in the solution phase by theoretical calculations, J. Phys. Chem. A 121 (2017)

4505-4516.

[45] Y. Izato, A. Miyake, Kinetic analysis of the thermal decomposition of liquid ammonium

nitrate based on thermal analysis and detailed reaction simulations, J. Therm. Anal. Carolim.

(2018), doi.org/10.1007/s10973-018-7322-8.

[46] P. Politzer and J. M. Seminario, Computational study of the structure of dinitraminic acid,

HN(NO2)2, and the energetics of some possible decomposition steps, Chem. Phys. Lett. 216

(1993), 348‑352.

Table 1

Table 1. Reactions and rate coefficients employed during the kinetic modeling of ionic decomposition. units are in cm^3 mol s cal.

No.	Reaction	k		
		A	n	ΔE_a
1	$ADN_I \rightleftharpoons ADN_{IIa}$	2.06×10^{12}	0.04	1472
2	$ADN_{IIa} \rightleftharpoons ADN_{IIb}$	1.73×10^{12}	0.00	2420
3	$ADN_{IIb} \rightleftharpoons ADN_{IIc}$	4.58×10^{12}	0.03	1382
4	$ADN_{IIc} \rightleftharpoons ADN_{IId}$	1.86×10^{12}	0.01	2072
5	$ADN_{IIa} \rightleftharpoons NH_4^+ + DN^-$	1.06×10^{14}	-0.13	8671
6	$ADN_{IIb} \rightleftharpoons NH_4^+ + DN^-$	4.66×10^{13}	-0.07	8224
7	$ADN_{IIc} \rightleftharpoons NH_4^+ + DN^-$	2.90×10^{13}	-0.24	4349
8	$ADN_I \rightleftharpoons NH_3 + HDN_I$	2.21×10^{13}	-0.01	15737
9	$ADN_{IIa} \rightleftharpoons NH_3 + HDN_{IIa}$	5.95×10^{13}	-0.24	23189
10	$ADN_{IIb} \rightleftharpoons NH_3 + HDN_{IIb}$	1.84×10^{14}	-0.24	20051
11	$ADN_{IIc} \rightleftharpoons NH_3 + HDN_{IIc}$	6.10×10^{15}	-0.24	27302
12	$ADN_I \rightleftharpoons AN + N_2O$	2.03×10^{11}	0.31	45903
13	$ADN_{IIa} \rightleftharpoons AN + N_2O$	5.48×10^{13}	0.39	47298
14	$ADN_{IIb} \rightleftharpoons AN + N_2O$	4.79×10^{13}	0.28	43791
15	$ADN_{IIc} \rightleftharpoons AN + N_2O$	1.97×10^{13}	0.44	46048
16	$ADN_{IId} \rightleftharpoons AN + N_2O$	1.76×10^{13}	0.46	49351
17	$NH_4^+ + DN^- \rightleftharpoons AN + N_2O$	1.54×10^2	3.40	36959
18	$ADN_I \rightarrow NH_4NNO_2\cdot + NO_2\cdot$	1.48×10^{15}	-0.03	39910
19	$NH_4NNO_2\cdot + NO_2\cdot \rightarrow ADN_I$	1.00×10^{12}	0	0
20	$ADN_{IIa} \rightarrow NNO_2NH_4\cdot + NO_2\cdot$	5.43×10^{13}	0.42	36223
21	$NNO_2NH_4\cdot + NO_2\cdot \rightarrow ADN_{IIa}$	1.00×10^{12}	0	0
22	$ADN_{IIb} \rightarrow NNO_2NH_4\cdot + NO_2\cdot$	1.02×10^{14}	0.28	33981
23	$NNO_2NH_4\cdot + NO_2\cdot \rightarrow ADN_{IIb}$	1.00×10^{12}	0	0
24	$ADN_{IIc} \rightarrow NNO_2NH_4\cdot + NO_2\cdot$	9.82×10^{15}	-0.34	33975
25	$NNO_2NH_4\cdot + NO_2\cdot \rightarrow ADN_{IIc}$	1.00×10^{12}	0	0
26	$ADN_{IId} \rightarrow NNO_2NH_4\cdot + NO_2\cdot$	5.85×10^{11}	1.07	35324
27	$NNO_2NH_4\cdot + NO_2\cdot \rightarrow ADN_{IId}$	1.00×10^{12}	0	0
28	$NH_4NNO_2\cdot \rightleftharpoons NNO_2NH_4\cdot$	3.36×10^{11}	0.01	-60
29	$NNO_2NH_4\cdot \rightleftharpoons N_2O + NH_3 + OH\cdot$	2.27×10^{10}	0.78	12828
30	$NNO_2^-\cdot + NH_4^+ \rightleftharpoons NH_4NNO_2\cdot$	1.00×10^{12}	0	0
31	$NNO_2^-\cdot + NH_4^+ \rightleftharpoons NNO_2NH_4\cdot$	1.00×10^{12}	0	0
32	$HNNO_2\cdot + NH_3 \rightleftharpoons NH_4NNO_2\cdot$	1.00×10^{12}	0	0

33	$NNO_2H\cdot + NH_3 \rightleftharpoons NNO_2NH_4\cdot$	1.00×10^{12}	0	0
34	$HDN_I \rightleftharpoons HDN_{IIa}$	2.47	3.44	25748
35	$HDN_{IIa} \rightleftharpoons HDN_{IIb}$	5.20×10^{12}	0.10	3332
36	$HDN_{IIb} \rightleftharpoons HDN_{IIc}$	6.79×10^{11}	0.07	20683
37	$HDN_{IIc} \rightleftharpoons HDN_{IId}$	3.36×10^{10}	1.08	4735
39	$HDN_{IId} \rightleftharpoons HDN_{IIa}$	4.33×10^{10}	0.06	19141
39	$HDN_I + HDN_I \rightleftharpoons HDN_{IIa} + HDN_{IIa}$	2.34×10^{-3}	3.56	5885
40	$HDN_{IIb} + HDN_{IIb} \rightleftharpoons HDN_{IIc} + HDN_{IIc}$	5.16×10^{-3}	3.61	-2098
41	$HDN_I \rightleftharpoons HNO_3 + N_2O$	1.35×10^{12}	0.33	36500
42	$HDN_{IIa} \rightleftharpoons HNO_3 + N_2O$	1.07×10^{12}	0.34	36681
43	$HDN_{IIb} \rightleftharpoons HNO_3 + N_2O$	1.24×10^{12}	0.38	35652
44	$HDN_{IIc} \rightleftharpoons HNO_3 + N_2O$	9.07×10^{9}	1.69	38416
45	$HDN_I + NO_3^- \rightleftharpoons DN^- + HNO_3$	1.00×10^{12}	0	0
46	$HDN_{IIa} + NO_3^- \rightleftharpoons DN^- + HNO_3$	1.00×10^{12}	0	0
47	$HDN_{IIb} + NO_3^- \rightleftharpoons DN^- + HNO_3$	1.00×10^{12}	0	0
48	$HDN_{IIc} + NO_3^- \rightleftharpoons DN^- + HNO_3$	1.00×10^{12}	0	0
49	$HDN_{IId} + NO_3^- \rightleftharpoons DN^- + HNO_3$	1.00×10^{12}	0	0
50	$HDN_I \rightleftharpoons HNNO_2 + NO_2\cdot$	398×10^{13}	0.08	36013
51	$HDN_{IIa} \rightleftharpoons NNO_2H + NO_2\cdot$	1.19×10^{12}	1.23	31147
52	$HDN_{IIb} \rightleftharpoons NNO_2H + NO_2\cdot$	3.22×10^{24}	-2.55	37480
53	$HDN_{IIc} \rightleftharpoons NNO_2H + NO_2\cdot$	7.31×10^{13}	1.07	31205
54	$HDN_{IId} \rightleftharpoons NNO_2H + NO_2\cdot$	1.34×10^{14}	0.34	31525
55	$HNNO_2\cdot \rightleftharpoons NNO_2H\cdot$	3.61×10^{-1}	3.68	20628
56	$HNNO_2\cdot + H_2O \rightleftharpoons NNO_2H + H_2O$	4.15×10^{1}	2.80	10005
57	$NNO_2H\cdot \rightleftharpoons N_2O + OH\cdot$	3.88×10^{12}	0.43	3996
58	$HNNO_2 + NO_2\cdot \rightleftharpoons ONONHNO_2$	4.38	2.89	1120
59	$ONONHNO_2 \rightleftharpoons NH(O)NO_2\cdot + NO\cdot$	3.91×10^{13}	-0.06	5864
60	$NH(O)NO_2\cdot \rightleftharpoons HNO + NO_2\cdot$	6.65×10^{13}	0.30	4095
61	$NNO_2H\cdot + NO_2\cdot \rightleftharpoons ONONN(OH)O$	8.55	2.99	-5374
62	$ONONN(OH)O \rightleftharpoons ONNO + HONO$	3.42×10^{12}	0.37	22261
63	$ONONN(OH)O \rightleftharpoons NO\cdot + ONNO_2H\cdot$	1.64×10^{13}	0.28	14412
64	$ONNO_2H\cdot \rightleftharpoons HONO + NO\cdot$	1.35×10^{13}	-0.02	364
70	$DN^- \rightleftharpoons NO_3^- + N_2O$	1.07×10^{12}	1.29	46994
71	$DN^- \rightarrow NNO_2^-\cdot + NO_2\cdot$	6.86×10^{14}	-0.09	41309
73	$NNO_2^-\cdot + NO_2 \rightleftharpoons ONONNO_2^-$	1.25×10^{1}	3.12	1720
74	$ONONNO_2^- \rightleftharpoons ONNO + NO_2^-$	1.41×10^{12}	0.24	17862

75	$ONNO + NO_2^- \rightleftharpoons NO_3^- + N_2O$	5.75×10^1	2.85	-2643
76	$ONNO \rightleftharpoons NO\cdot + NO\cdot$	6.20×10^{12}	0.22	6679
77	$NNO_2^- + t\text{-}ONONO_2 \rightleftharpoons NO_3^- + N_2O + NO_2$	6.70	3.07	706
78	$NNO_2^-\cdot + NO \rightleftharpoons ONNNO_2^-$	3.89×10^3	2.48	-1780
79	$ONNNO_2^- \rightleftharpoons NO_2^- + N_2O$	7.44×10^{12}	0.29	20452

Table 2

Table 2. Calculated enthalpies (kJ mol^{-1}) for the formation of species associated with ADN decomposition. The estimated absolute value of 386.3 kJ mol^{-1} for $\Delta_f H°(H^+)$ [39].

	$\Delta_f H°_{gas,calc}$	$\Delta_{solv} H°_{calc}$	$\Delta_f H°_{aq,calc}$
ADN$_I$	18.3	-64.5	-46.2
ADN$_{IIa}$	21.6	-69.2	-47.6
ADN$_{IIb}$	19.4	-65.1	-45.7
ADN$_{IIc}$	26.3	-70.6	-44.3
ADN$_{IId}$	26.3	-69.8	-43.6
HDN$_I$	107.9	-21.8	86.1
HDN$_{IIa}$	123.80	-18.6	105.2
HDN$_{IIb}$	121.40	-19.4	102.0
HDN$_{IIc}$	130.6	-22.2	108.4
HDN$_{IId}$	124.0	-18.5	105.4
DN$^-$	-129.7	-217.2	39.3
NH$_4$NNO$_2$·	148.3	-46.8	101.5
NNO$_2$NH$_4$·	136.3	-49.9	86.4
HNNO$_2$·	222.1	-15.2	206.9
NNO$_2$H·	232.0	-14.0	218.0
NNO$_2^-$·	49.6	-246.0	189.9
ONONHNO$_2$	125.7	-18.8	106.9
ONONN(OH) O	163.0	-20.1	142.8
ONONNO$_2^-$	-23.8	-215.4	147.1
ONNO	247.7	-9.6	238.1

Table 3

Table 3. Calculated thermodynamic data for species associated with ADN decomposition.

SPECIES	$\Delta_f H^\circ_{liq,calc}$	$S^\circ_{liq,calc}$	C_P [J K^{-1} mol^{-1}]						
	[kJ mol^{-1}]	[J mol^{-1} K^{-1}]	300	400	500	600	800	1000	1500 K
ADN$_I$	-46.2	414.42	130.27	151.33	169.76	185.26	208.75	225.19	249.44
ADN$_{IIa}$	-47.58	406.40	129.6	151.04	169.64	185.19	208.69	225.12	249.37
ADN$_{IIb}$	-45.68	410.41	129.92	151.25	169.79	185.33	208.81	225.22	249.44
ADN$_{IIc}$	-44.33	411.47	130.41	151.61	170.06	185.50	208.85	225.18	249.36
ADN$_{IId}$	-44.33	417.20	131.42	152.32	170.57	185.84	208.89	225.06	249.13
HDN$_I$	86.14	347.60	90.52	107.67	121.43	132.14	146.92	156.21	168.41
HDN$_{IIa}$	105.18	341.19	92.71	109.81	123.32	133.74	148.01	156.92	168.64
HDN$_{IIb}$	102.04	344.91	93.02	109.92	123.32	133.68	147.91	156.82	168.57
HDN$_{IIc}$	108.39	343.65	93.79	110.69	123.95	134.18	148.22	157.02	168.65
HDN$_{IId}$	105.44	326.58	87.08	105.56	120.29	131.74	147.58	157.45	169.89
DN$^-$	39.33	325.33	83.88	99.61	112.14	121.67	134.25	141.56	150.05
NH$_4$NNO$_2 \cdot$	101.48	332.62	83.96	97.77	110.43	121.50	138.99	151.74	171.33
NNO$_2$NH$_4 \cdot$	86.38	348.79	92.99	106.76	119.30	130.24	147.53	160.18	179.67
HNNO$_2 \cdot$	206.89	289.37	58.10	66.40	73.21	78.63	86.35	91.46	98.66
NNO$_2$H$\cdot$	218.01	276.08	57.33	66.29	73.35	78.81	86.39	91.32	98.33
NNO$_2^- \cdot$	189.94	267.54	47.47	55.13	61.27	65.92	71.99	75.48	79.47
ONONHNO$_2$	106.90	350.07	98.82	114.28	126.44	135.91	149.16	157.66	169.06
ONONNO$_2$H	142.88	345.92	101.97	117.81	129.77	138.83	151.23	159.07	169.61
ONONNO$_2^-$	106.40	339.18	91.18	106.02	117.35	125.82	136.93	143.40	150.92

Figure 1
Click here to download high resolution image
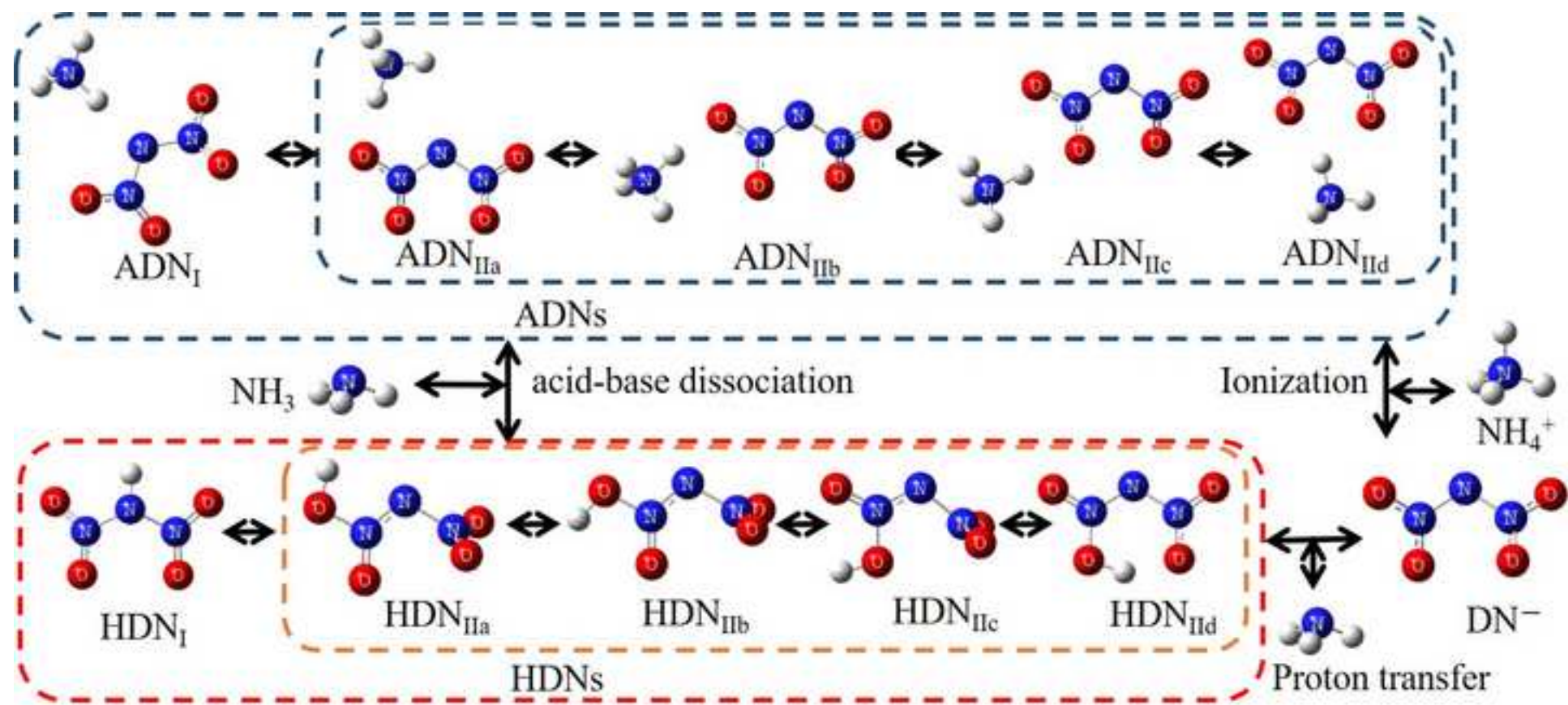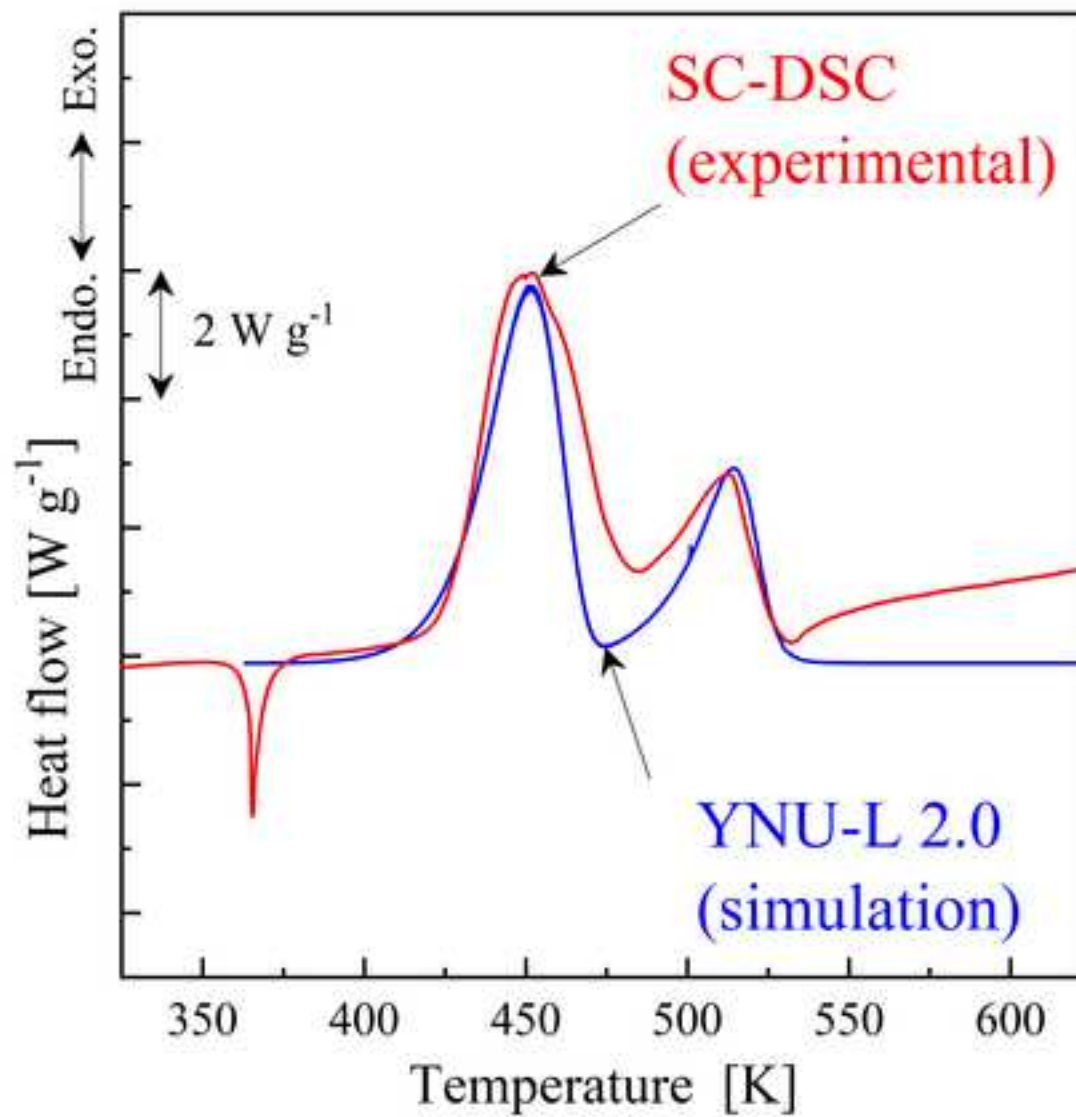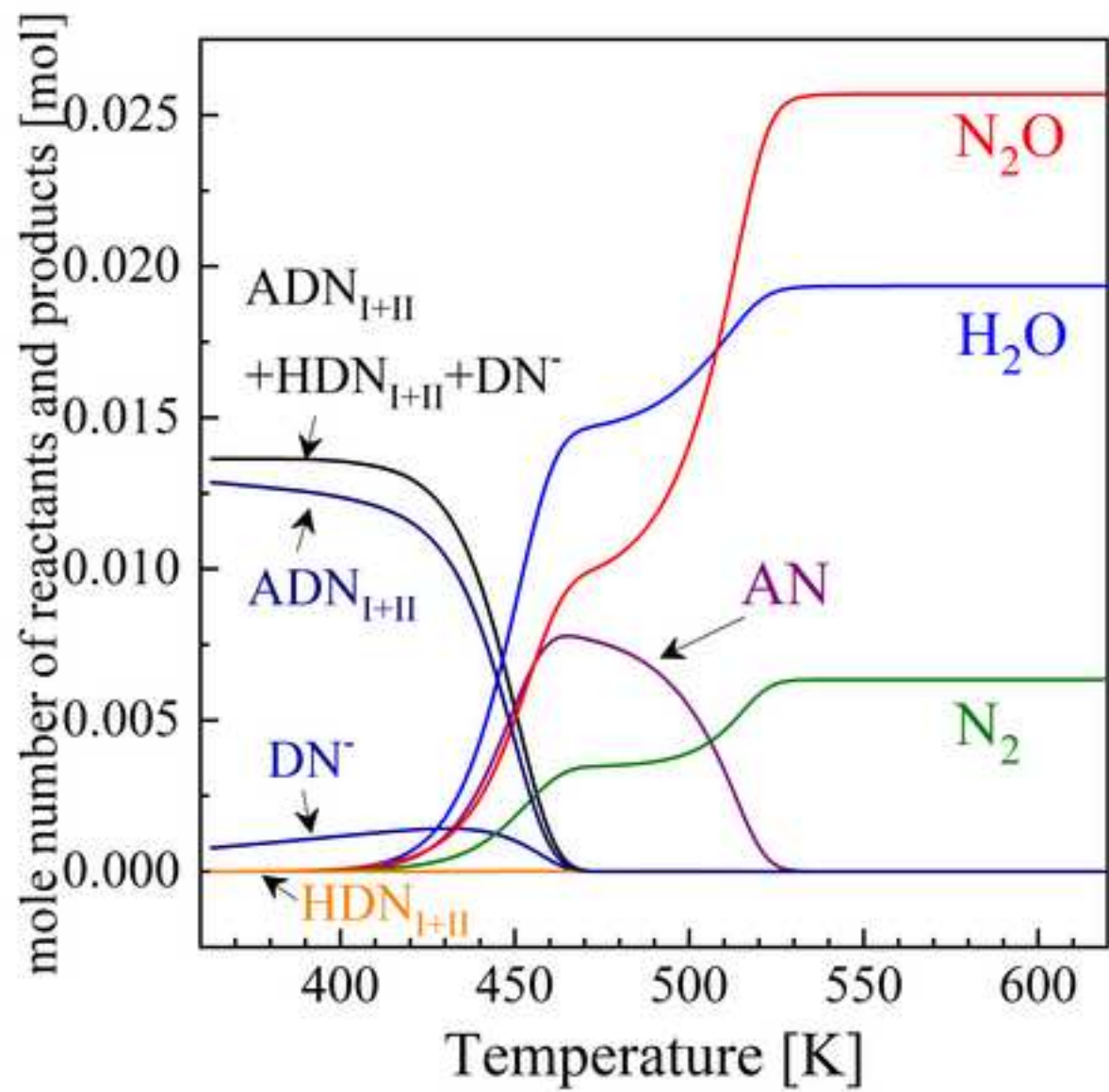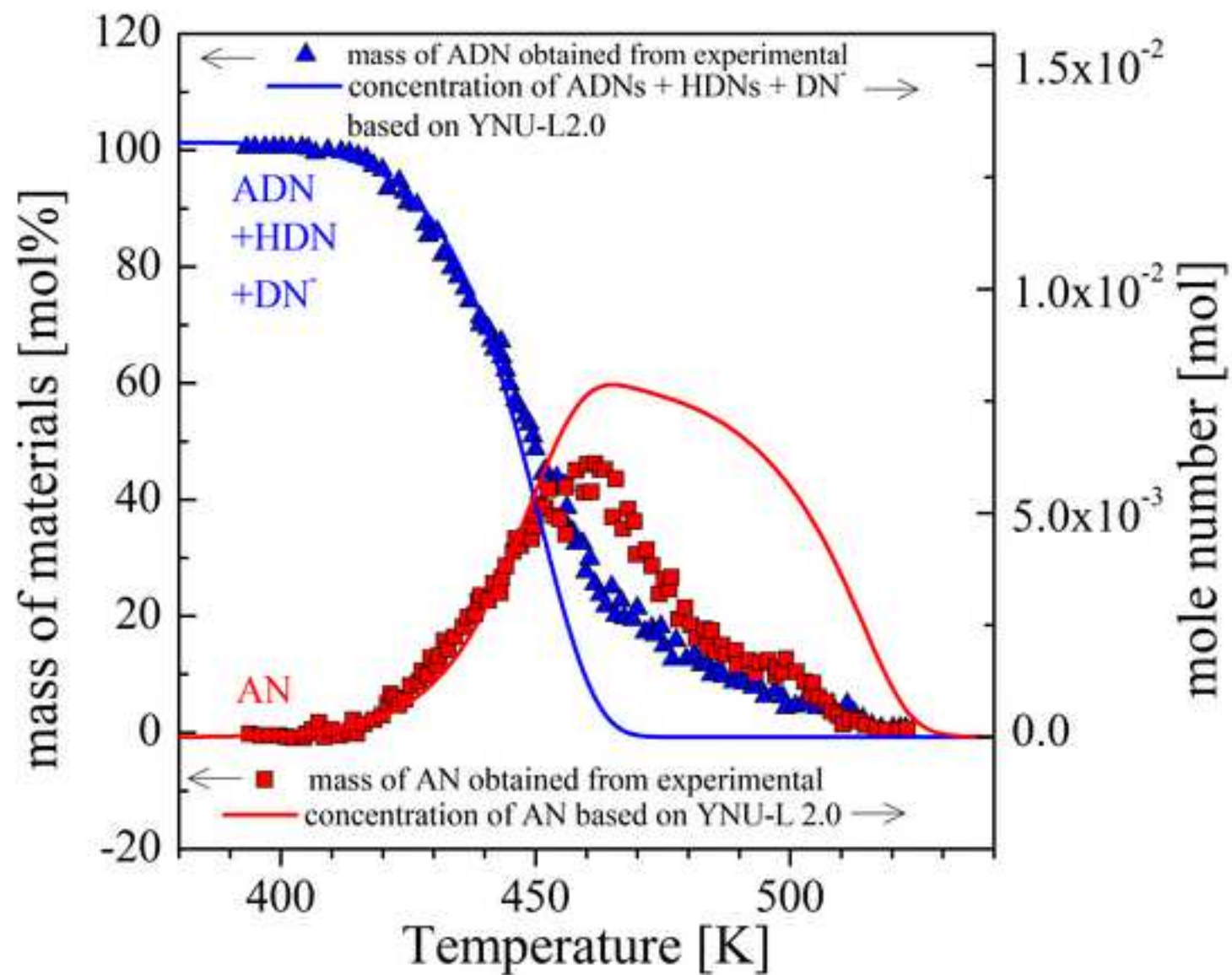
Figure 5-1
Click here to download high resolution image

a) NO_2

$ADN_{IIc} =$
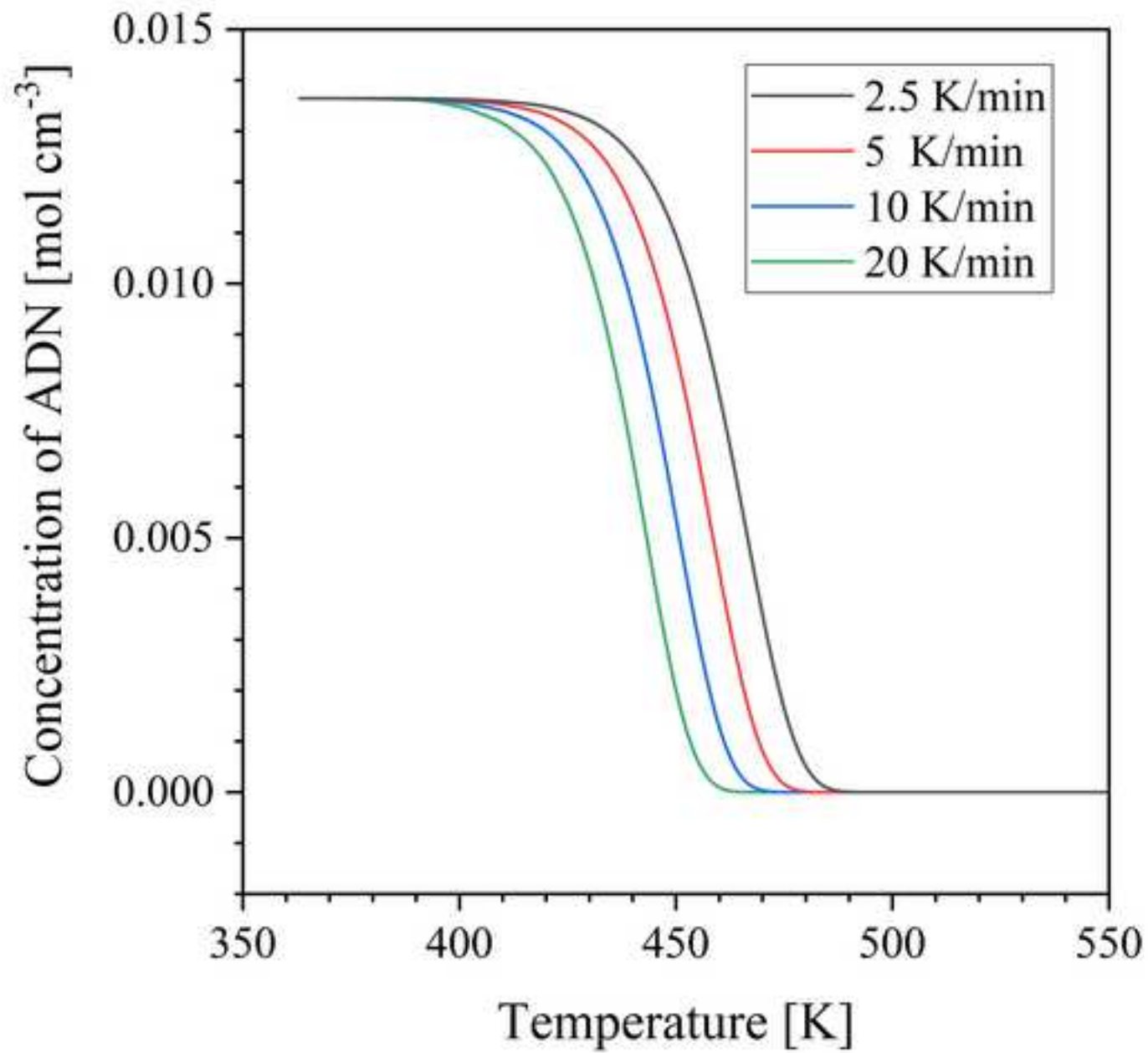$NNO_2NH_4 + NO_2$
$ADN_{IIb} =$
$NNO_2NH_4 + NO_2$

$HDN_{IIc} =$
$NNO_2H + NO_2$
$DN^- =$
$NNO_2^- + NO_2$

$NO_2 + NO_2 =$
$t\text{-}ONONO_2$

$NH_2 + NO_2 =$
NH_2NO_2

$NO_2 + OH => HNO_3$

rate of production of NO_2 / mol cm^{-3} s^{-1}

Temperature / K
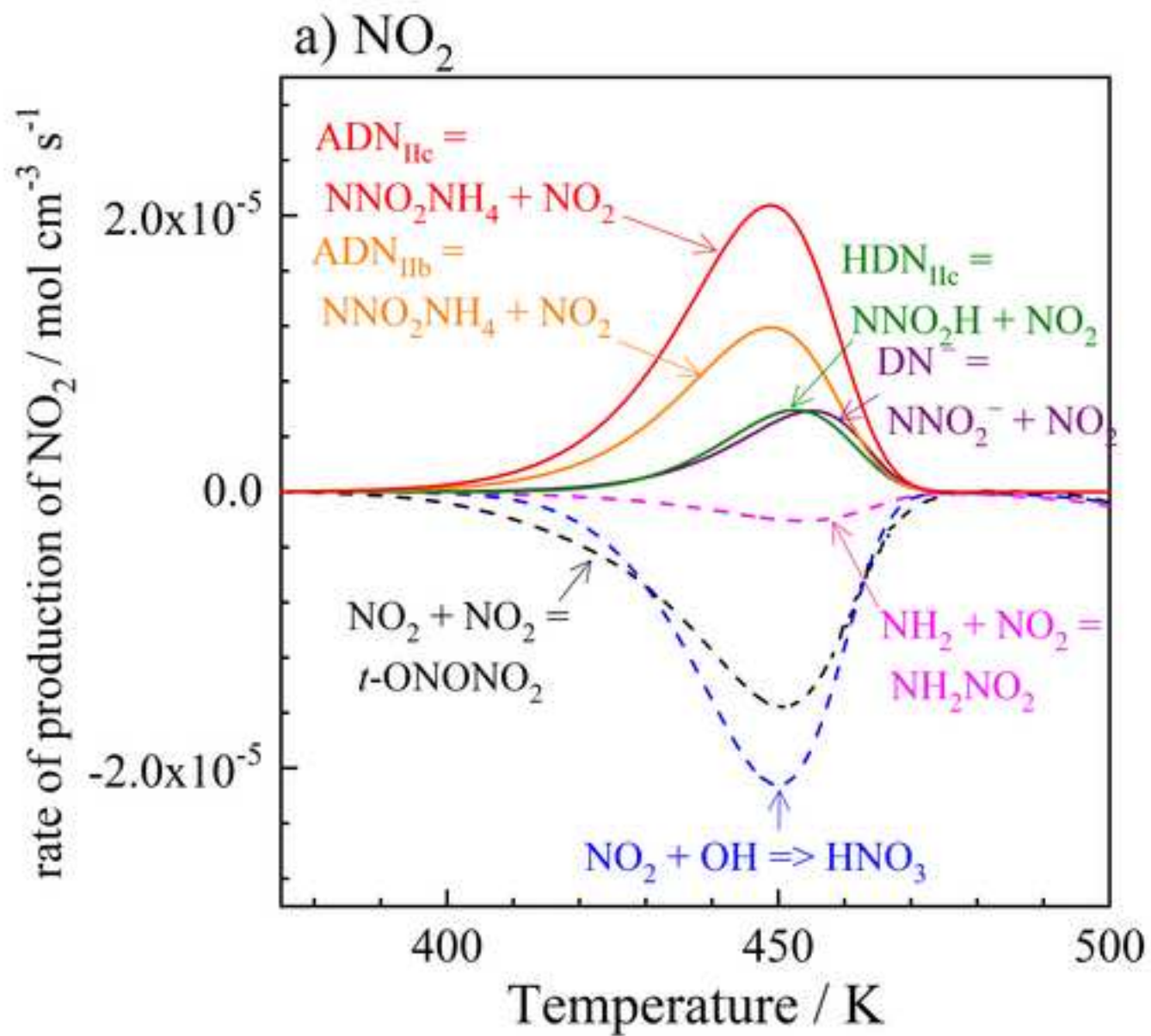
Figure 5-2
Click here to download high resolution image

b) OH

$NNO_2NH_4 =$
$NH_3 + OH + N_2O$

$NNO_2H =$
$OH + N_2O$

$NH_3 + OH =>$
$NH_2 + H_2O$

$NO_2 + OH => HNO_3$

rate of production of OH / mol cm^{-3} s^{-1}

Temperature / K
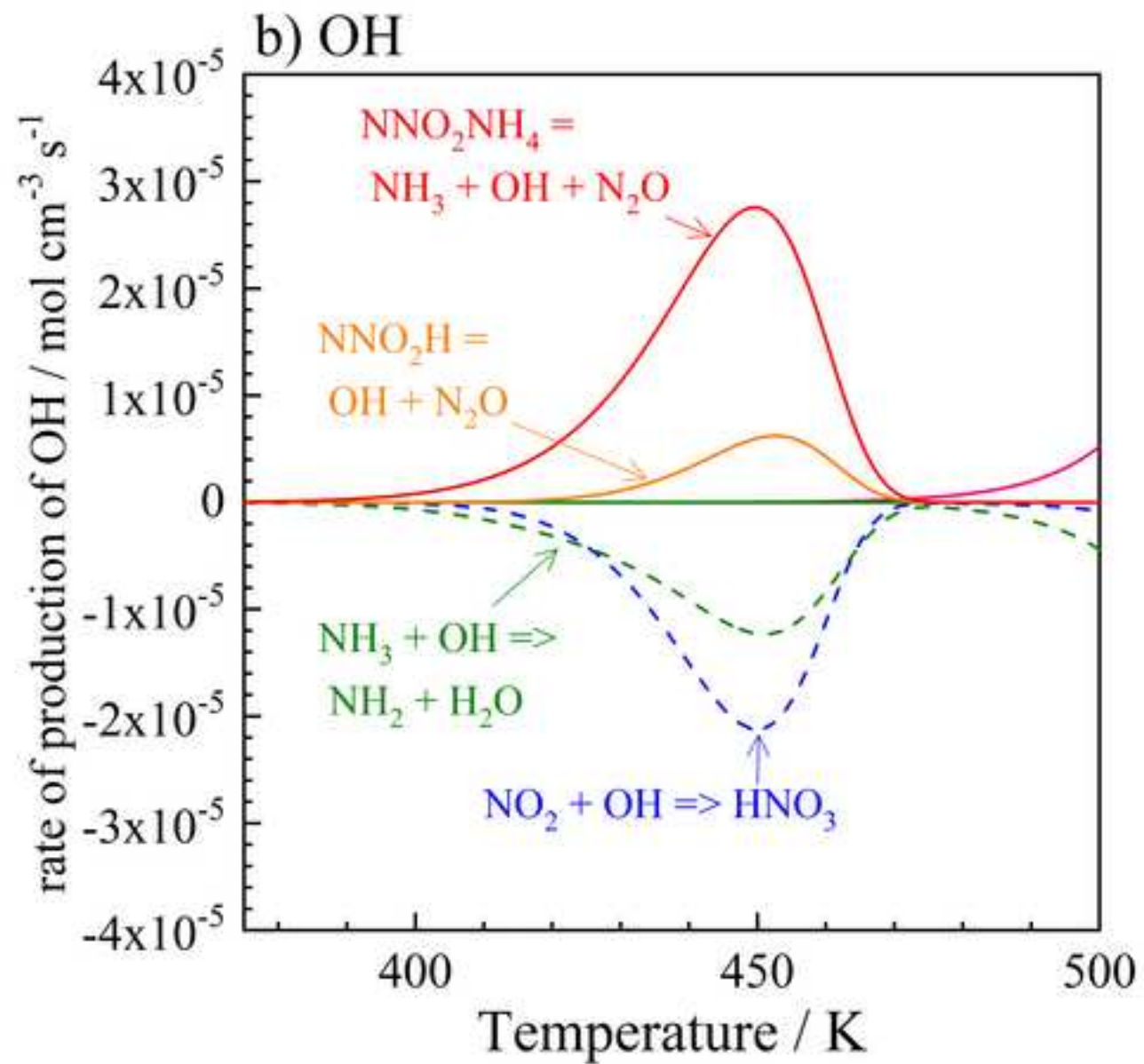
Figure 6
Click here to download high resolution image
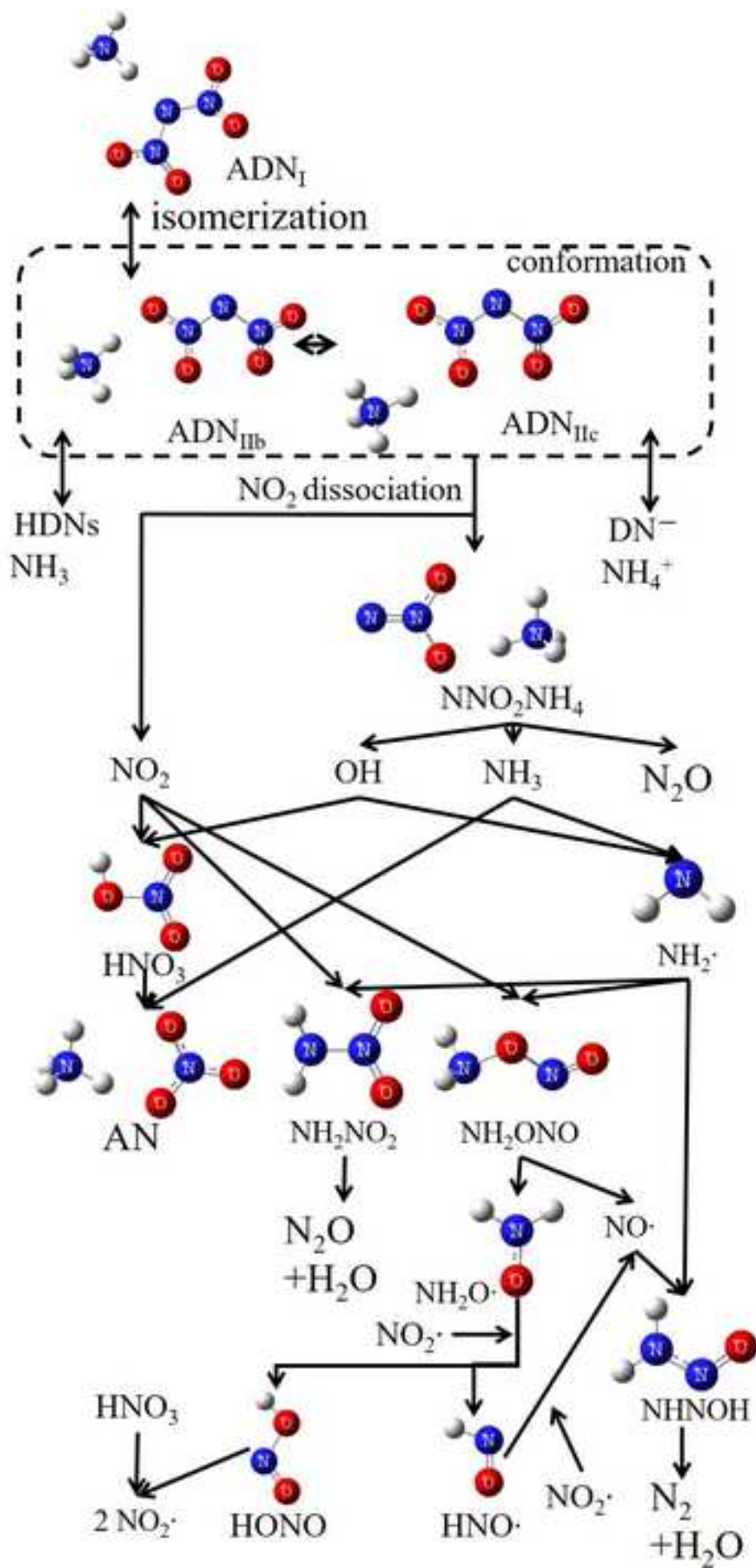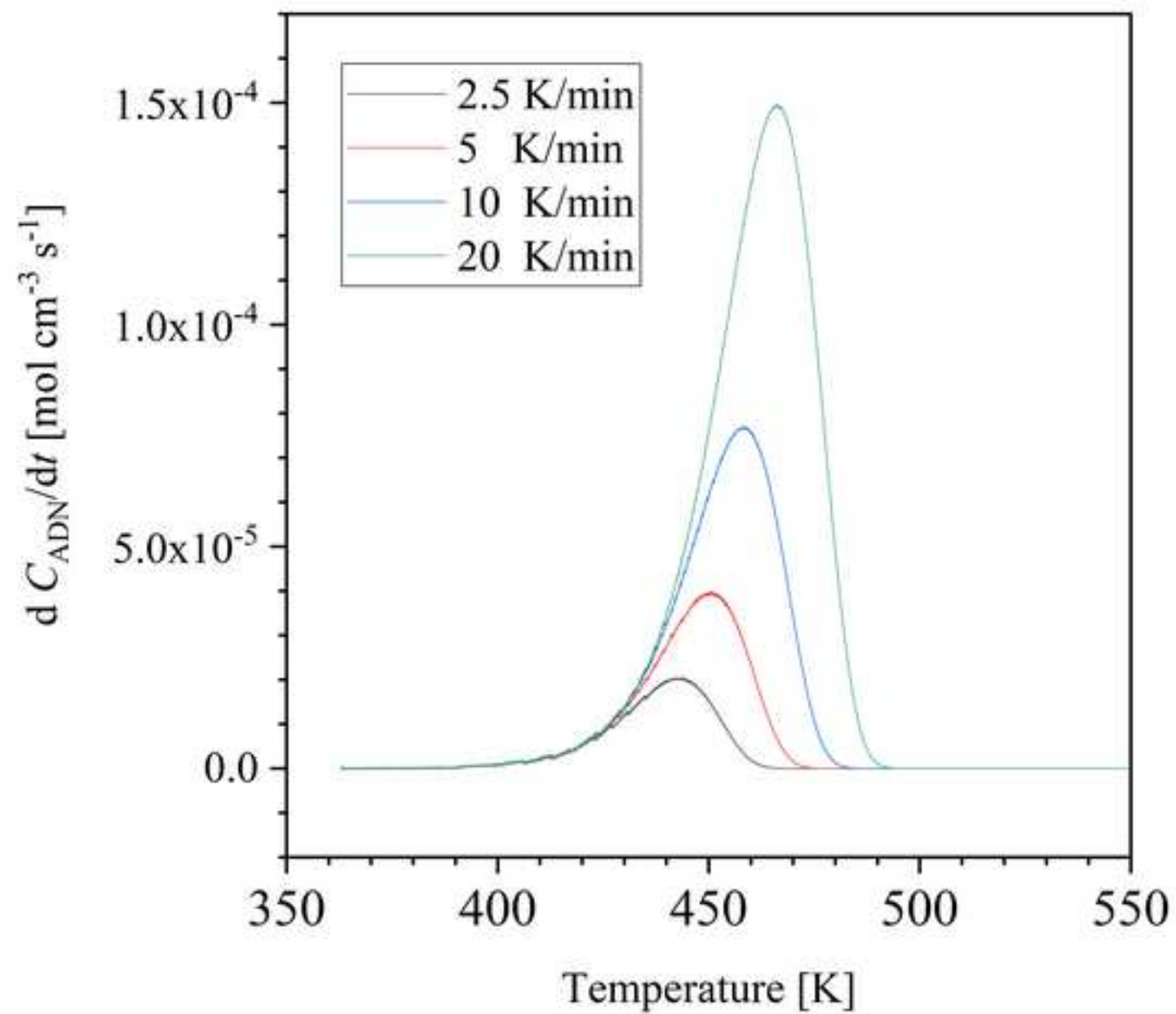
Figure S3
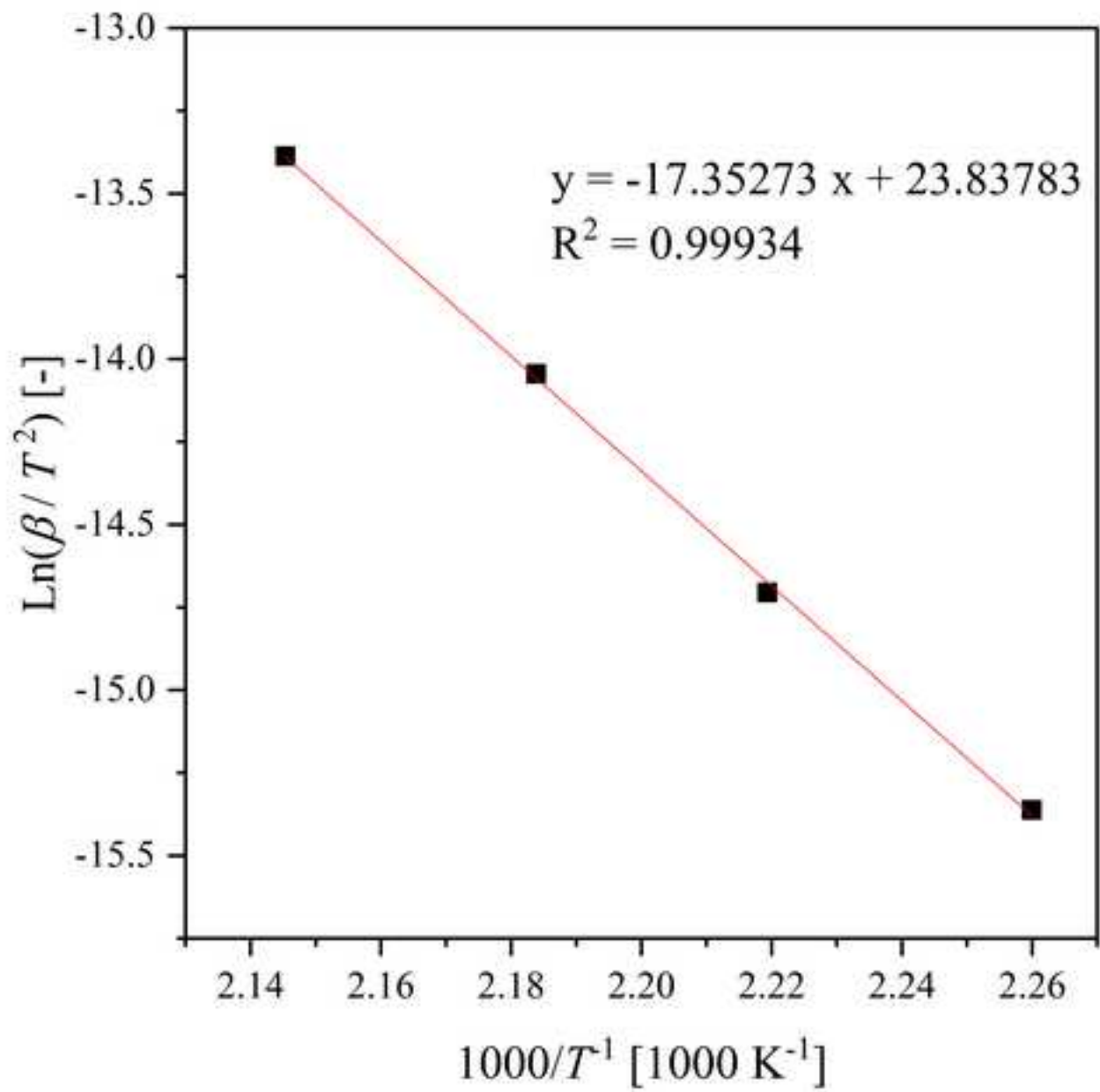
$y = -17.35273\,x + 23.83783$

$R^2 = 0.99934$

Axis labels: $\mathrm{Ln}(\beta\,/\,T^{2})\;[\text{-}]$ versus $1000/T^{-1}\;[1000\;\mathrm{K}^{-1}]$
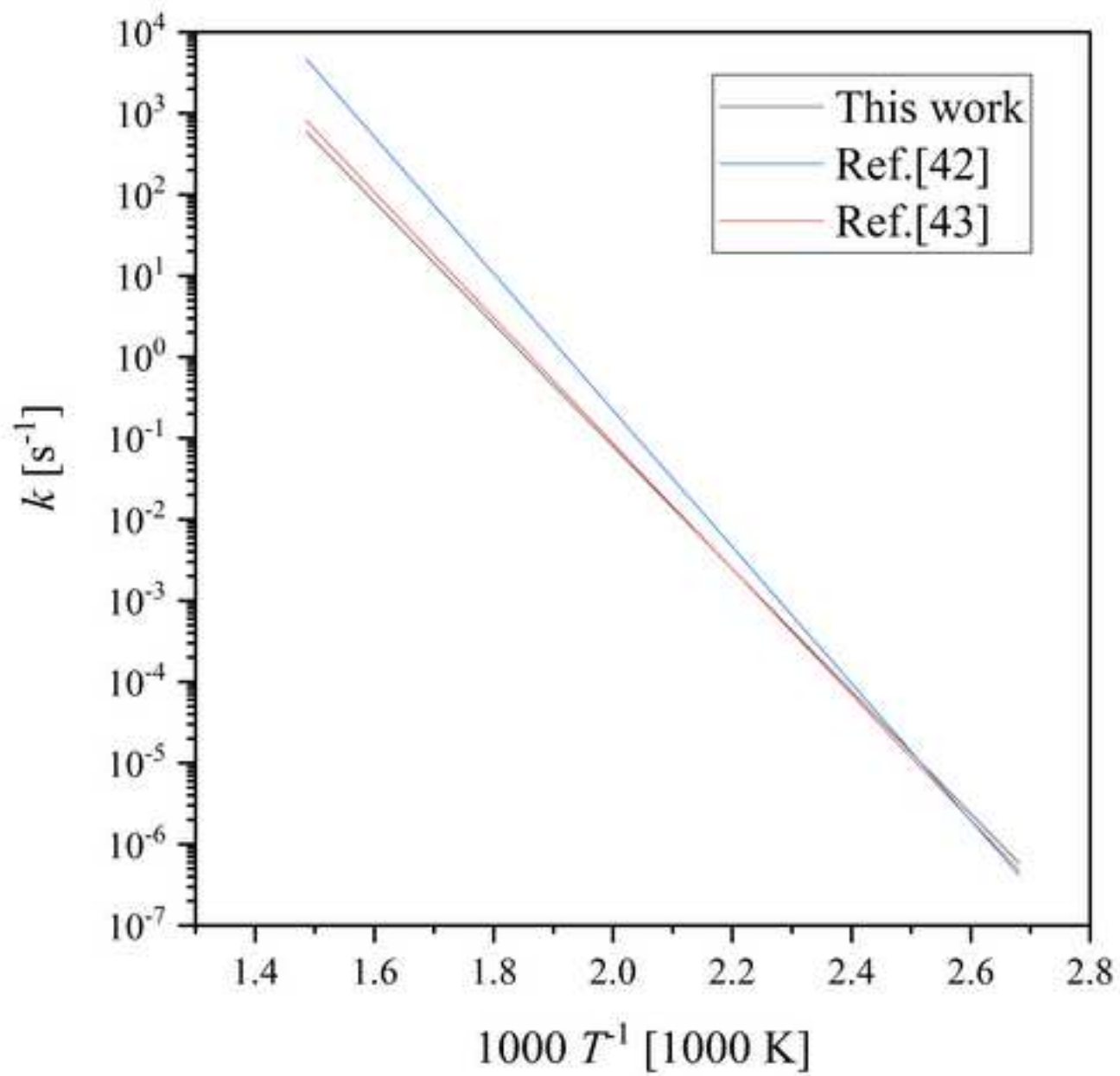
Supplementary Material
Click here to download Supplementary Material: YNU-L20_thermo for adn.dat

Supplementary Material

Supplementary Material
Click here to download Supplementary Material: SI.docx